Locking and Unlocking the Molecular Spin Crossover Transition

Paulo S. Costa, Daniel P. Miller, Alpha T. N'Diaye, Peter A. Dowben, Xin Zhang, Paulo S Costa, James Hooper, Daniel P Miller, Alpha T N'Diaye, Sumit Beniwal, et al.

DOI: 10.1002/((please add manuscript number))

Article type: Communication

Locking and Unlocking the Molecular Spin Cross-Over Transition

Xin Zhang, Paulo S. Costa, James Hooper, Daniel P. Miller, Alpha T. N'Diaye,* Sumit Beniwal, Xuanyuan Jiang, Yuewei Yin, Patrick Rosa, Lucie Routaboul,* Mathieu Gonidec, Lorenzo Poggini, Pierre Braunstein,* Bernard Doudin,* Xiaoshan Xu,* Axel Enders,* Eva Zurek,* Peter A. Dowben**

X. Zhang, P. S. Costa, S. Beniwal, X. Jiang, Dr. Y. Yin, Dr. X. Xu, Dr. A. Enders, Dr. P. A. Dowben

Department of Physics and Astronomy, University of Nebraska, Lincoln, Nebraska 68588-0299, U.S.A.

E-mail: pdowben@unl.edu, xiaoshan.xu@unl.edu

Dr. J. Hooper

Department of Theoretical Chemistry, Faculty of Chemistry, Jagiellonian University, Krakow, Poland 30-060

E-mail: james.hooper@uj.edu.pl

D. P. Miller, Dr. E. Zurek

Department of Chemistry, University of Buffalo, Buffalo, New York 14260-3000 U.S.A.

E-mail: ezurek@buffalo.edu

Dr. A. T. N'Diaye

Advanced Light Source, Lawrence Berkeley National Laboratory, Berkeley, CA, 94720 U.S.A.

Email: atndiaye@lbl.gov

P. Rosa, M. Gonidec, L. Poggini

CNRS, Univ. Bordeaux, ICMCB, UPR 9048, F-33600 Pessac, France.

Email: patrick.rosa@icmcb.cnrs.fr

Dr. L. Routaboul, Dr. P. Braunstein

Université de Strasbourg, CNRS, CHIMIE UMR 7177, Laboratoire de Chimie de Coordination, 4 rue Blaise Pascal, 67081 Strasbourg, France.

Email: lroutaboul@unistra.fr, braunstein@unistra.fr

Dr. B. Doudin

University of Strasbourg, CNRS, IPCMS UMR 7504, 23 rue du Loess, 67034 Strasbourg, France.

Email: Bernard.Doudin@ipcms.unistra.fr

Dr. A. Enders

Physikalisches Institut, Universität Bayreuth, 95440 Bayreuth, Germany.

Email: Axel.Enders@uni-bayreuth.de

Keywords: Spin crossover transition, X-ray excited spin states, spin state locking, substrate interactions, zwitterion complexes.

ABSTRACT. The Fe(II) spin crossover complex [Fe{$H_2B(pz)_2$}$_2$(bipy)] (pz = pyrazol-1-yl, bipy = 2,2'-bipyridine) can be locked in a largely low spin state configuration over a temperature range that includes temperatures well above the thermal spin crossover temperature of 160 K. This locking of the spin state is achieved for nanometer thin films of this complex in two distinct ways; through substrate interactions with dielectric substrates such as SiO_2 and Al_2O_3, or in powder samples by mixing with the strongly dipolar zwitterionic *p*-benzoquinonemonoimine $C_6H_2(\cdots NH_2)_2(\cdots O)_2$. Remarkably, we find in both cases that incident X-ray fluences then restore the [Fe{$H_2B(pz)_2$}$_2$(bipy)] moiety to an electronic state characteristic of the high spin state at temperatures of 200 K to above room temperature, i.e. well above the spin crossover transition temperature for the pristine powder and well above the temperatures characteristic of light- or X-ray-induced excited spin-state trapping. Heating slightly above room temperature allows the initial locked state to be restored. These findings, supported by theory, show how the spin crossover transition can be manipulated reversibly around room temperature by appropriate design of the electrostatic and chemical environment.

The spin crossover (SCO) phenomenon, in several classes of 3*d* transition metal compounds, relates to the temperature-induced transition between a low spin (LS) diamagnetic state of the metal ion to a high-spin (HS) paramagnetic state, usually stable at a higher temperature.[1,2] The SCO transition can also be triggered by light or pressure changes, making it an ideal system for multi-functional devices at the molecular level, in particular, if the transition is

accompanied by a change of conductivity,[3-16] with the perspective of reaching low voltage GHz switching.[17] For molecular memory applications, where non-volatility is required, there is a strong need to identify and control mechanisms to lock, unlock and switch the molecular spin state at a given temperature, ideally around 300 K, if devices applications are envisioned. Unfortunately, most reported SCO molecules exhibit transition temperatures significantly below 300 K.[18]

Creating bi-stability at a given temperature can be obtained by a light stimulus, making the HS state (high-temperature state) metastable at low temperatures where the LS state normally prevails. For a metastable high spin state with a very long lifetime retention, such light-induced excited spin state trapping (LIESST) [4,9,19-35] and soft X-ray induced excited spin state trapping (SOXIESST) [35-38] are limited to temperatures significantly below the SCO transition, that is to say below 50-60 K. For bi-stability at higher temperatures exceeding the SCO transition, it is necessary to 'lock' the low temperature LS state into a metastable state. Such a suppression of the spin state transition has been observed for [Fe(1,10-phenanthroline)$_2$(NCS)$_2$],[11] and [Fe{$H_2B(pz)_2$}$_2$(bipy)] (pz = pyrazol-1-yl, bipy = 2,2'-bipyridine),[13,35,39-41] molecules or ultra-thin films interacting with a metallic substrate, with a resulting mixed spin state dominated by the LS state at high temperatures.[13,35,40] This basically implies a substrate-induced "locking" of the spin state.

The question arises whether the spin state of SCO complexes can be locked into a metastable state far away from the transition temperature, then unlocked and switched as needed, and possibly even reset to the metastable state. The possibility of manipulating the spin state of an ultrathin film is suggested by the fact that the signature of the spin crossover transition, in X-ray absorption spectroscopy,[42] is not always in lock step with the magnetometry. Furthermore, unlocking and changing the spin state of an ultrathin spin crossover molecular film was achieved by STM tip manipulation over Au substrates [6] or by inserting a dielectric substrate like CuN,[11] although performed at temperatures below the SCO transition temperature.

Here, we exploit our initial findings that interactions with an electrically-active ferroelectric substrate, specifically residual dipoles at their surface, can impact the state of SCO molecular films,[41] to achieve the desired room-temperature switchable spin state. We extend this concept here by studying the mixture of SCO with dipolar molecules, investigating how such electrostatically-active neighbors can influence the ligand field around the metal center, and therefore impact the stability of its magnetic state. A key advantage of dipoles is that they can possibly be oriented by an external electric field (with ferroelectrics as the asymptotic case of collective behavior), opening the possibility to control the SCO magnetic state with an electric field. Such giant magnetoelectric coupling at the molecular level is what is missing for inorganic materials applications in the field of multiferroics. In this paper, we show that the spin state transition of $[Fe\{H_2B(pz)_2\}_2(bipy)]$, where pz = tris(pyrazol-1-yl)-borohydride and bipy = 2,2'-bipyridine (hereafter **1**, **Figure 1**) can be suppressed through interactions with

dielectric substrates as well as with quinonoid zwitterion molecular additives (hereafter **2**, Figure 1), so that they are locked in a predominantly LS state at room temperature, far beyond their SCO transition temperature of 160 K. We then show that unlocking and switching of the spin state is achieved by incident X-ray fluences (schematically summarized in **Figure 2**). Reversibility of this transition is obtained by a mild heating of the material (by typically 40 K), bringing back the system to a dominant locked LS state (Figure 2). We, therefore, take advantage of the expected sensitivity of the Fe ion to the local environment,[3,6-7,9-16,41,43,44] and illustrate how the spin state of **1** can be manipulated at room temperature through engineered interactions with neighbor molecules or substrates.

The spin state of molecule 1, in powder form and as a 5 nm thin films on SiO_2, may be extracted from the X-ray absorption spectra, such as those in **Figure 3**, as a function of temperature and as a function of time. In the LS state of molecule **1**, the 3*d* electrons occupy the t_{2g} orbitals in pairs leaving the e_g empty.[30,32,35,40-42,45] This is observable in the shown $2p_{3/2}$ (Fe L_3) X-ray absorption spectra as a major e_g peak at about 708 eV (Figure 3). In the HS state, the e_g orbitals are partly populated with the t_{2g} set subsequently partly depopulated, which corresponds in the XAS spectra at the Fe L_3 ($2p_{3/2}$) edge to a decrease of the peak intensity at 708 eV and an increase of the corresponding t_{2g} peak at about 706.5 eV.

The powder of molecule **1** shows the characteristic shift of the t_{2g} and e_g peak intensities, in a narrow temperature range around 150 K, revealing the thermally-induced SCO. The 5 nm thin film of **1** on SiO_2 does not display such a thermally-induced transition and instead the

initial Fe L_3 ($2p_{3/2}$) X-ray absorption spectra observed at low temperatures remain unchanged up to room temperature. This is seen from the blue curve in Figure 3(b), which was taken at room temperature. The initial spectra are similar to that of the powder of molecule **1** at low temperature in that the e_g peak shows by far of the highest intensity so that it must be concluded that the film is mostly in an LS state at 290 K.

In a similar fashion, the initial spectra of 5 nm thin films of **1** on SiO_2 at 200 K, 300 K, 345 K and of 30 nm thin films on another dielectric substrate, Al_2O_3, show spectral characteristics very similar to the LS state (**Figure 4**). It is thus concluded that similarly to thin films of **1** on Au (111),[13,35,39,40] interactions with SiO_2 and Al_2O_3 dielectric substrates also tend to pin the SCO molecular thin films of **1** into the LS state up to 345 K.

Interestingly, the time evolution of the spectra during exposure of the films to X-rays during the XAS measurements at a constant temperature around 290 K, detailed in Figures 4b and 5, show a systematic behavior reminiscent of the SOXIESST "unlocking" of the LS state, allowing a transition to the HS state, although occurring well above the thermal transition temperature. When increasing scan speeds to a few seconds per spectrum (at the expense of resolution and signal to noise ratio), the evolution of the X-ray absorption spectra of 5 nm thin films of **1** on SiO_2 at 200 K can be monitored. It resembles the temperature evolution of the SCO transition, as seen in **Figure 3**, by exhibiting a decrease in the e_g-like peak and an increase in the unoccupied t_{2g}-like peak. This indicates that the spin state of **1** has evolved

towards an HS state as a function of exposure time to the soft X-rays, at a constant temperature. Similar results have been obtained at higher temperatures for 5 nm thick films of **1** on SiO_2 and 30 nm thick films on Al_2O_3.

Qualitatively, the soft X-ray induced spin crossover transition increases in rate with increasing temperature, achieving nearly complete HS state occupancy for 1 within roughly 13 minutes of exposure at 200 K (Figure 4a), 4-5 minutes at 300 K (Figure 4b) and 3 minutes at 345 K (Figure 4c). The "empty t_{2g} / empty e_g" ratio is an empirical approximation indicator to extract the occupancy of the HS state, in good agreement with theoretical expectations,[42] and used in **Figure 5** to establish the evolution of the soft X-ray-induced transition to the HS state with time, as a function of temperature. Even though the SOXIESST-like process, leading to occupancy of a metastable HS state, is gradual (Figure 4), the evolution of this process proceeds far more quickly than the traditional SOXIESST, as seen for the powdered molecule **1** below 50 K, and as plotted in Figure 6. This increasing rate of this SOXIESST process with increasing temperature, above the traditional thermal spin crossover transition temperature, suggests that this "unlocking" is a thermally-activated process. Applying an Arrhenius equation to the observed rates, and by assuming a constant pre-exponential factor, an activation energy of 60±7 meV/molecule can be estimated. This value (of approximately 60 meV) is close to enthalpy variation associated with the spin transition, which has been determined to be in the region of 80 meV.[30]

The resulting excited HS state, or "unlocked" HS state, is stable for at least one hour at room temperature without X-ray irradiation. In comparison, changing the spin state of a SCO molecular complex, with LIESST and SOXIESST at temperatures below 50-60 K, for molecules like **1** or [Fe(bpz)$_2$(phen)] (bpz = dihydrobis(pyrazolyl)borate, phen = 1,10-phenanthroline) results in the complex remaining trapped in a metastable state with a lifetime up to days.[24,31,32,35,46-48] However, when the ultrafast photoexcitation spectroscopy is performed at room temperature, the photogenerated high spin state complex is a transient species with extremely short lifetimes of picoseconds to nanoseconds,[26,49-53] although lifetimes up to 36 ms [54,55] have been observed. In other words, the transitions we report here result in an HS state that is at least five orders of magnitude more stable as a function of time.

It should be emphasized that this soft X-ray-induced transition is reversible, as illustrated in **Figure 6**. With a mild annealing, only slightly exceeding room temperature, molecule **1** relaxes back to the LS initial state. This reversibility excludes photodecomposition as a possible mechanism since photodecomposition effects would be largely temperature independent.

Several mechanisms for the unlocking of the substrate pinning of thin films of molecule **1** and subsequent transition to a majority HS state should be considered. The activation energy of 60±7 meV is too small (and too close to the energy associated with expected enthalpy change for the spin crossover transition) to be associated with the breaking of chemical bonds,

so charge rearrangement and configuration changes remain likely mechanisms for the observed high temperature soft X-ray-induced transition to an HS state. Neither SiO_2 nor molecule **1** assemblies are expected to be good conductors.[42] Under soft X-ray fluences, photoemission will occur and charge can build up at the interface, resulting in local electric fields that could facilitate a transition of the spin states of the SCO molecule.[6,7,10,11,13] This tends to run contrary to the observations that the process is an activated process, as conductivity in SiO_2 increases with increasing temperature. Changes to the local charge population, distortions of the ligand or metal coordination sphere, as a result of local changes in charge, are also possible mechanisms for the induced spin state switching.[18] These mechanisms are difficult to model, presently, as the interaction of molecule **1** with SiO_2 or Al_2O_3 is not known. Thus, to gain further insights into the possible cause of the environmental influence on the delicate energetics of the SCO transition, we investigated the phase stability of molecule 1 in the presence of other electrically and chemically mildly active neighbor molecules.

Here we use strongly dipolar molecules, mixed with molecules of 1, to manipulate the spin state transition. We used molecule **2** as an additive, as such zwitterions possess a dipole moment in the region of 10 Debyes. When combining the SCO complex **1** with **2**, the SCO molecule HS state is significantly suppressed, see **Figure 7**. Specifically, less than 40% of the molecules are in the HS state at room temperature, as determined by X-ray absorption spectroscopy. This leads to a majority occupancy of the LS state from 79 K to 340 K, which corresponds to temperatures that are well above the thermal SCO transition temperature. This

suppression of the HS state occupancy has been found empirically to be most pronounced for mixtures of **1** and **2** in a 1:2 molar ratio, and is in agreement with magnetometry measurements (SI, Fig. S1). We can infer, from the X-ray absorption spectra, that the HS state occupancy, before soft X-ray illumination, is significantly higher than for thin films of **1** on SiO_2 and Al_2O_3, as discussed above.

Similarly to the molecular thin films of **1**, the irradiation of the powder mix, by soft X-rays, leads to an increase in the HS state occupancy, as inferred from the X-ray absorption spectra (Figure 7). Again, using the "empty t_{2g} / empty e_g" ratio, observed in the thermal evolution of molecule **1**, in the bulk state as discussed above and shown in Figure 3a, the evolution of the occupancy of the HS state under soft X-rays irradiation can be estimated, as summarized in Figure 7c. Although the initial occupancy in the HS state is higher at 300 K than at 79 K, as is evident from the X-ray absorption spectra (Figures 8a and 8b, respectively), the growth rate of the HS state fraction is larger when the temperature is increased (Figure 8c).

The increased HS state occupancy at 300 K, due to soft X-rays fluences, can be returned back to a majority LS state after a mild temperature annealing up to 340 K, as seen in **Figure 8**. The annealing leads to rapid relaxation of a significant fraction of **1** back to the original "locked" LS state.

The experiments consistently showed that dipolar surfaces as well as dipolar molecular additives to **1** lock molecules mostly in the LS state at room temperature, where they can be switched into the HS state with X-ray fluences. Since the investigated samples are in powder form, with at least micron sized grains, exceeding the X-rays attenuation length in the 100-200 nm range, substrate effects may be excluded. Trapped charges, at the substrate interface, can thus be safely ruled out, but electrostatic potentials have to be considered in computational models aiming at determining the underlying mechanism of the locking and unlocking of the molecular spin state.

We have carried out density functional theory calculations to elucidate the mechanism of locking and unlocking of the molecular spin state using this mechanism. Both **1** and **2** have non-homogeneous electrostatic potentials (ESP) and appreciable dipole moments, as shown in **Figure 9**. This suggests that there should be energetically preferred orientations when **2** interacts with **1**. Subtle changes in the orientation of the $H_2B(pz)_2$ ligands lead to two energetically competitive isomers of molecule **1** (see **Figure 10a**); the B-H group reaches toward the nearby bipyridine ligand in geometry **1-a**, but it instead tilts toward the other $H_2B(pz)_2$ ligand in geometry **1-b**. The **1-a** geometry is only slightly more stable, by 1 kcal/mol (43 meV) than the **1-b** geometry in the gas-phase, and the low-spin electronic spin state is energetically favored in both geometries, with the PBE+D3 functional, at zero temperature (supplementary materials, Table S1). The more stable 1-a geometry corresponds with the isomer that has been reported in crystal structures of 1 below 300 K.[46-47] The computed Gibb's free energies of the LS and HS configurations of **1-a** and **1-b** confirm that

the HS electronic state becomes, relatively speaking, energetically more favored at higher temperature, by about 4-5 kcal/mol between 0 K and 298 K. This is qualitatively consistent with the observed preference for the HS state above 160 K in the pure SCO (Supplementary material, Table S1).

The most distinguishing difference between the **1-a** and **1-b** geometries is, arguably, their molecular dipole moments, as shown in Figure 10a, since the dipole moment of the **1-b** geometry (8.7 Debye) is nearly double that of the **1-a** geometry (4.7 Debye). We confirmed that an external electric dipole field that is aligned parallel to the molecular dipole moment can indeed shift the relative energies in favor of the **1-b** geometry and increase the HOMO-LUMO gap. For example, a field strength of 2.57×10^{9} $V \cdot m^{-1}$ increases the HOMO-LUMO gap of the LS state by 0.25 eV and favors the 1-b geometry by 4 kcal/mol, which represents a 5 kcal/mol shift in comparison to the gas-phase values. Conversely, electric dipole fields that align against the dipole moment of **1** can further favor geometry **1-a**. This suggests that such fields could affect the relative populations of the two geometries at room temperature or, less drastically, influence the molecular geometries and curvature of the potential energy surface around the **1-a** and **1-b** geometries, thereby affecting the structure's dynamics. For example, the N1···N2 distances is 0.03 Å shorter in the **1-b** geometry than in the **1-a** geometry, so an increased preference for the former geometry in the presence of favorable dipole-dipole interactions, as is hinted at from the simulations, would result in an overall shorter N1···N2 distance.

Considering now a mix of **1** with zwitterion **2**, we illustrate in **Figure 10(b-d)** how the electronic density around **1** is perturbed by **2** when the latter is adsorbed at different orientations. As a rule of thumb, the electron density around **1** is increased near the positively charged -NH_2 groups of **2**, while the electron density is reduced near the carbonyl groups of **2** (see Figure 10d); this is suggestive of dipole-dipole interactions. The most stable orientation of **2** binding to **1**, via non-covalent interactions (shown in Figure 10b for the **1-b** geometry), is when **2** is placed in the pocket between the bipyridine and $H_2B(pz)_2$ ligands, which does indeed match up a relatively electron-poor of each fragment's ESP profile with an electron-rich region of the other fragment's ESP profile. The binding energy of **2** to **1** at this binding site was computed to be -16 kcal/mol (Supplementary material, Table S1). When molecule 2 was rotated by 180 degrees, so that the direction of its dipole moment is reversed, the binding energy dropped to less than -8 kcal/mol. This supports that, as expected, **1** interacts to some extent with the dipole moment of the zwitterionic molecule **2**. Furthermore, we noticed that when the position of **2** is moved along the $H_2B(pz)_2$ ligand to introduce an N-H···H-B contact between **2** and the **1-b** geometry, the N1···N2 distance on that $H_2B(pz)_2$ ligand decreases by 0.04 Å. This illustrates that weak bonding interactions between **1** and **2**, such as through the N-H···H-B interactions, can also subtly influence the coordination spheres around the Fe center. A similar effect was reported for $[Fe(pic)_3]^{2+}$.S, where pic=2-picolylamine and S a solvent molecule, where changing the hydrogen-bonded solvent altered dramatically the occurrence of spin crossover.[56]

The interactions between **2** and **1**, that have been described so far, correspond to interactions that leave the intramolecular bonding of each fragment intact as sketched for model 3 in **Figure 11** and do not consider covalent bonding between **1** and **2**. We note, however, that the most stable configuration of **2** binding to molecule **1** in our density functional theory simulations is when **2** substitutes a hydrogen atom at each $–BH_2-$ site on **1**, through a hydroboration-like reaction, to form covalent B-O bonds like those shown in model **4** (see Figure 11). Such a transformation does require a substantial displacement of the substituted H atom and it is not obvious how the packing/interactions within a crystal structure might affect it, but the computed binding energy of **2** to **1** to form **4** is roughly -37 kcal/mol at $T = 0$ K, which amounts to a two-fold to three-fold stabilization over configuration **3**. The LS configuration of **4** is favored over the HS configuration more than it is in **1** alone, by 3-4 kcal/mol at 298 K. The formation of **4** also affects the coordination spheres around the Fe center, shortening, for example, the N1···N2 distance by 0.03 Å in the HS state. The increased preference for the LS state and shorter N1···N2 distances in **4** are both also consistent with the electronic and physical changes that we suggest above to accompany the overall preference for the LS state that is experimentally observed. Thus, the possibility of such a hydroboration-like reaction could also, alongside the dipole-dipole interactions, explain the observed preference for the LS state. We leave the aromaticity of the zwitterion moiety of **4** as undetermined, as indicated by the absence of any double bond in Figure 11, as there is presently no experimental confirmation as to whether the nonaromatic character of **2** is retained or the chemical modifications on **2** may restore aromaticity of the carbon ring, as

has been proposed elsewhere.[61] The model of **4** has C-C bond lengths of 1.4 Ångstroms throughout the ring, which is close to the value in benzene.

As shown in the SI, the presence of a B-O bond in model **4** gives rise to a low-intensity B-O stretching mode in the simulated Raman spectrum at 957 cm^{-1}, which is in close proximity to a new peak at 954 cm^{-1} observed in the experimental Raman spectra of the 1:2 molar ratio samples. The general agreement of both the simulated model **4** and model **3** spectra with the experimental spectrum is limited, in part because the computational models do not consider crystal packing nor solid state effects. Nonetheless, the computed frequency of the B-O stretching mode complements the computed thermodynamic preference for the formation of B-O bonds, and suggests that model **4** may be a representative for the species formed in experiment. However, calculation of activation barriers for the formation of **4** and X-ray diffraction data that can be compared with those obtained experimentally but future work is required to confirm the viability of model **4**.

Calculations on molecular models of 2 interacting with **1**, therefore, suggest several mechanisms through which 2 may be helping to lock molecule **1** in an LS electronic state near room temperature. A dipole electric field can alter the potential energy surface of molecule **1**, for example by altering the relative stabilities of the **1-a** and **1-b** geometries, and local dipole-dipole interactions between **2** and **1**, like intermolecular N-H···H-B interactions, can promote shorter N1···N2 distances in molecule **1**. The changes in charge displacement are

intimately connected to chemical interactions between **2** and **1**, which can also affect the geometric and electronic properties of **1**. However, the versatile ways in which zwitterion **2** can bind to **1** help explain why experimental procedures, e.g. the solvent choice, have such a profound effect on the fraction of **1** locked in the LS state. However, the discussion of such effects is beyond the scope of this paper.

It is well-known that the spin state of complexes like **1** is highly susceptible to even minor perturbations of the ligand chemistry,[43,44] and this is consistent with earlier reports of *permanent* substrate-induced spin state locking as discussed. The significance of this study is thus in the identification of a strategy to lock, unlock and switch the spin state of a spin-crossover complex around room temperature. Specifically, the Fe(II) spin crossover molecule **1**, which is usually in the HS state at temperatures above 160 K was stabilized in a metastable LS state through interactions either with a supporting dielectric substrate or with strongly dipolar additives to **1**. This metastable LS state was in both cases unlocked through soft X-ray absorption, triggering a transition to the HS state at room temperature. This process was fully reversible. From this, together with first principles calculations and the fact that there is no report of a similar effect on non-polar surfaces, we infer that dipolar effects are at least to some extend key to the reversible manipulation of the molecular spin state.

What is remarkable is that until now low temperatures were mandatory for efficient photoswitching with the LIESST effect, and, as such, were incompatible with room

temperature applications, though room temperature photoconductance changes in a spin crossover system have been observed.[58] This work on the molecular spin state manipulation shows that nonvolatile pinning of the spin state is possible at temperatures significantly exceeding the spin transition, proposing an alternative to synthetic design for achieving room temperature applications of SCO materials. Physical mechanisms for changing the spin state at room temperature exist. The soft X-ray fluence that leads to an electronic structure characteristic of the high spin state may explain why soft X-ray and other light fluences may result in a spin crossover transition temperature that differs from that measured by magnetometry, as reported elsewhere.[31,42,59] The potential barrier of the X-ray stimulated spin state change process is seen to be more readily accessible at higher temperatures but at the expense of phase stability. The extent of this interplay needs further investigation.

This work also revealed the need for further chemical engineering of the energetic of interactions of SCO molecules with their neighbors. The binding(s) of zwitterions with an SCO complex greatly affects the percentage of spin crossover molecules locked in the LS state, without affecting how much can be excited with soft-X-rays to the HS state. Theory suggests that chemically different interactions can be the cause of this. The control of one particular spin state occupancy, i.e. the engineering of the fraction of one spin or another, through chemistry, and the subsequent manipulation of that spin state means that a range of nonvolatile molecular memory devices could be anticipated corresponding to the molecular equivalent of a "level shifter" semiconductor device. Of key importance is to note that the spin cross-over transition temperature of an isolated spin cross-over complex might be well

below room temperature, but if the spin state can be "locked", the complex could be effective as a molecular magneto-electric. This locking of the spin state can be enabled by substrate interactions as well as chemical interactions with a dipolar molecule, like the zwitterion discussed above. Indeed a thermal spin crossover critical temperature, well below ambient, is preferred as long as the spin state can still be altered by extrinsic stimulus at room temperature. Key to the applicability of molecular magneto-electric is realization of the lifetime that can be maintained in each spin state at room temperature. We believe that this study establishes promising strategies to manipulate the spin state transition in SCO molecules and will help to design room temperature switchable organic magnets.

Experimental Section

Experimental:

Molecule 1 was synthesized according to the literature.[32] This electrically neutral molecule was thermally evaporated on various dielectric substrates, and we typically fabricated 5 nm thick molecular films on SiO_2 and 30 nm thick molecular thin films on Al_2O_3. The SCO transition temperature measured by magnetometry was found, with bulk material, to be about 160 K, in agreement with the literature.[30,32,35,40-42,45] Molecule **2** was synthesized as described,[60-63] and combined with 1: samples were prepared by weighing powders of **1** and **2**

in the desired molar ratio and mixing them together while dry. The resulting mixture of **1** and **2** was then immersed in isopropyl alcohol and placed in an ultrasonic bath for 20 min. and then the solvent was evaporated. This procedure resulted in a mixture of **1** and **2** with the majority of SCO molecules locked in the low spin state (as is evident in magnetometry and as discussed below). The resulting material also exhibits a spin crossover transition, leading to an increase in the HS state population by 5 to 10%, but remaining far from the nearly 100% occupancy in the HS state, as is observed in **1** alone. The molar ratio 1/2 of **1**:**2** was chosen for the studies here because, over many combinations, it resulted in the largest fraction of molecules in the LS state, ca. 60% from X-ray absorption measurements, at temperatures above 160 K.

The X-ray absorption spectroscopy (XAS) measurements were performed at the bending magnet beamline 6.3.1, at the Advanced Light Source at Lawrence Berkeley National Laboratory. The photon flux is on the order of 10^{11} photons/sec/0.1%BW.[64] The temperature was stabilized within ±1 degree Kelvin. Positive circular polarized X-ray was used. Total electron yield (TEY) mode was used to measure the absorption of the Fe L_3 and L_2 edges. The X-ray beam was blanked or moved to a fresh sample spot when necessary to avoid artifacts through uncontrolled exposure.

Supporting Information

Supporting Information is available from the Wiley Online Library or from the author.

Acknowledgements

This research was supported by the National Science Foundation through NSF-Chem 1565692 [XZ, PAD] and the Nebraska MRSEC (DMR-1420645) [PC, SB, YY, XJ, XX]. We also acknowledge support from the Agence Nationale de la Recherche Labex NIE 11-LABX-0058_NIE within the Investissement d'Avenir program ANR-10-IDEX-0002-02. Partial financial support of the Agence Nationale de la Recherche and IdEx Bordeaux within Investissement d'Avenir program (ANR-10-IDEX-03-02) and the International Center for Frontier Research in Chemistry (icFRC, Strasbourg) are also gratefully acknowledged. Use of the Advanced Light Source, Lawrence Berkeley National Laboratory, was supported by the U.S. Department of Energy under contract no. DE-AC02-05CH11231. J.H. acknowledges an 'Outstanding Young Scientist' scholarship from the Ministry of Science and Higher Education in Poland for financial support. D. M. was funded by the NSF (HRD-1345163). We acknowledge support from the Center of Computational Research at SUNY Buffalo.

Received: ((will be filled in by the editorial staff))
Revised: ((will be filled in by the editorial staff))
Published online: ((will be filled in by the editorial staff))

References

a) A. B. Author 1, C. D. Author 2, *Adv. Mater.* **2006**, *18*, 1; b) A. Author 1, B. Author 2, *Adv. Funct.*

Mater. **2006**, *16*, 1.

[1] O. Kahn, In: Molecular Magnetism, Eds. Wiley-VCH.: New York, August **1993**.

[2] P. Gütlich, Y. Garcia, H. A. Goodwin, *Chem. Soc. Rev.* **2000**, *29*, 419.

[3] D. Aravena, E. Ruiz, *J. Am. Chem. Soc.* **2012**, *134*, 777.

[4] N. Baadji, S. Sanvito, *Phys. Rev. Lett.* **2012**, *108*, 217201.

[5] E. J. Devid, P. N. Martinho, M. V. Kamalakar, I. Šalitroš, U. Prendergast, J.-F. Dayen, V. Meded, T. Lemma, R. González-Prieto, F. Evers,; Keyes, T. E M. Ruben, B. Doudin, S. J. van der Molen, *ACS Nano.* **2015**, *9*, 4496.

[6] T. G. Gopakumar, F. Matino, H. Naggert, A. Bannwarth, F. Tuczek, R. Berndt, *Angew. Chem. Int. Ed.* **2012**, *51*, 6262.

[7] W. Kuch, M. Bernien, *J. Phys. Cond. Matt.* **2017**, *29*, 023001.

[8] C. Lefter, V. Davesne, L. Salmon, G. Molnár, P. Demont, A. Rotaru, A. Bousseksou, *Magnetochemistry* **2016**, *2*, 18.

[9] E. Ludwig, H. Naggert, M. Kalläne, S. Rohlf, E. Kröger, A. Bannwarth, A. Quer, K. Rossnagel, L. Kipp, F. Tuczek, *Angew. Chem. Int. Ed.* **2014**, *53*, 3019.

[10] T. Mahfoud, G. Molnár, S. Cobo, L. Salmon, C. Thibault, C. Vieu, P. Demont, A. Bousseksou, *A. Appl. Phys. Lett.* **2011**, *99*, 053307.

[11] T. Miyamachi, M. Gruber, V. Davesne, M. Bowen, S. Boukari, L. Joly, F. Scheurer, G. Rogez, T. K. Yamada, P. Ohresser, E. Beaurepaire, W. Wulfhekel, *Nat. Comm.* **2012**, *3*, 938.

[12] F. Prins, M. Monrabal-Capilla, E. A. Osorio, E. Coronado E. H. S. van der Zant, *J. Adv. Mater.* **2011**, *23*, 1545.

[13] A. Pronschinske, Y. Chen, G. F. Lewis, D. A. Shultz, A. Calzolari, M. B. Nardelli, D. B. Dougherty, *Nano Lett.* **2013**, *13*, 1429.

[14] A. Rotaru, I. y. Gural'skiy, A. G. Molnar, L. Salmon, P. Demont, A. Bousseksou, *Chem. Commun.* **2012**, *48*, 4163

[15] A. Rotaru, J. Dugay, R. P. Tan, I. A. Gural'skiy, L. Salmon, P. Demont, J. Carrey, G. Molnar, M. Respaud, A. Bousseksou, *Adv. Mater.* **2013**, *25*, 1745.

[16] E. Ruiz, *Phys. Chem. Chem. Phys.* **2014**, *16*, 14

[17] J. J. Trasobares, D. Vuillaume, D. Theron, N. Clement, *Nat. Commun.* **2016**, *7*, 12850

[18] M. Khusniyarov, *M. Chem. Eur. J.* **2016**, *22*, 15178.

[19] K. Bairagi, O. Iasco, A. Bellec, A. Kartsev, D. Li, J. Lagoute, C. Chacon, Y. Girard, S. Rousset, F. Miserque, Y. J. Dappe, A. Smogunov, C. Barreteau, M.-L. Boillot, T. Mallah, V. Repain, *Nature Comm.* **2016**, *7*, 12212.

[20] L. Capes, J.-F. Létard, O. Kahn, *Chem. – Eur. J.* **2000**, *6*, 2246.

[21] M. Duriska, B. S. Neville, M. B. Moubaraki, J. D. Cashion, G. J. Halder, K. Chapman, W. C. Balde, J.-F. Létard, K. S. Murray, C. J. Kepert, S. R. Batten, *Angew. Chem. Int. Ed.* **2009**, *48*, 2549.

[22] T. Gopakumar, G. M. Bernien, H. Naggert, F. Matino, C. F. Hermanns, A. Bannwarth, S. Mühlenberend, A. Krüger, D. Krüger, F. Nickel, W. Walter, R. Berndt, W. Kuch, F. Tuczek, *Chem. – Eur. J.* **2013**, *19*, 15702.

[23] P. Gütlich, H. A. Goodwin, Spin Crossover—An Overall Perspective. In: Spin Crossover in Transition Metal Compounds I; Gütlich, P., Goodwin, H. A., Eds. *Topics in Current Chemistry*; Springer Berlin Heidelberg, **2004**; 1.

[24] J.-J. Lee, H.-s. Sheu, C.-R. Lee, J.-M. Chen, J.-F. Lee, C.-C. Wang, C.-H. Huang, Y. J. Wang, *Am. Chem. Soc.* **2000**, *122*, 5742.

[25] J. Létard,-F. P. Guionneau, L. Goux-Capes, Towards Spin Crossover Applications. In Spin Crossover in Transition Metal Compounds III P. Gütlich,, Goodwin, H. A., Eds.; Topics in Cur-rent Chemistry; Springer Berlin Heidelberg, **2004**, 221.

[26] J. F. Létard, P. Guionneau, O. Nguyen, J. S. Costa, S. Marcén, G. Chastanet, M. Marchivie, L. Goux-Capes, *Chem. Eur. J.* **2005**, *11*, 4582.

[27] J. F. Létard, *F. J. Mat. Chem.* **2006**, *16*, 2550.

[28] J.-F. Létard, G. Chastanet, P. Guionneau, C. Desplanches, Optimizing the Stability of Trapped Metastable Spin States. In Spin-Crossover Materials, M. A. Halcrow, Ed.; John Wiley & Sons Ltd, **2013**, 475.

[29] M. Marchivie, P. Guionneau, J. A. Howard, K. G. Chastanet, J.-F. Létard, A. E. Goeta, D. J. Chasseau, *Am. Chem. Soc.* **2002**, *124*, 194.

[30] N. Moliner, L. Salmon, L. Capes, M. C. Muñoz, J.-F. Létard, A. Bousseksou, J.-P. Tuchagues, J. J. McGarvey, A. C. Dennis, M. Castro, R. Burriel, J. Real, *A. J. Phys. Chem. B.* **2002**, *106*, 4276.

[31] H. Naggert, A. Bannwarth, S. Chemnitz, T. von Hofe, E. Quandt, F. Tuczek,, *Dalton Trans.* **2011**, *40*, 6364.

[32] T. Palamarciuc, J. Oberg, C. F. El Hallak, C. F. Hirjibehedin, M. Serri, S. Heutz, J.-F. Létard, P. Rosa, *J. Mater. Chem.* **2012**, *22*, 9690.

[33] O. Sato, J. Tao, Y.-Z. Zhang, *Angew. Chem. Int. Ed.* **2007**, *46*, 2152.

[34] J. Tao, H. Maruyama, O. J. Sato, *Am. Chem. Soc.* **2006**, *128*, 1790.

[35] B. Warner, J. C. Oberg, T. G. Gill, F. El Hallak, C. F. Hirjibehe-din, Serri, M. S. Heutz, M.-A. Arrio, Sainctavit, P. M. Manni-ni, G. Poneti, R. Sessoli, P. J. Rosa, *Phys. Chem. Lett.* **2013**, *4*, 1546.

[36] M. Bernien, H. Naggert, L. M. Arruda, L. Kipgen, F. Nickel, J. Miguel, C. F. Hermanns, A. Krüger, D. Krüger, E. Schierle, E. Weschke, F. Tuczek, W. Kuch, *ACS Nano.* **2015**, *22 (9)*, 8960.

[37] D. Collison, C. D. Garner, C. M. McGrath, J. F. W. Mosselmans, M. D. Roper, J. M. W. Seddon, E. Sinn, N. A. Young, *J. Chem. Soc. Dalton Trans.* **1997** 4371.

[38] V. Davesne, M. Gruber, T. Miyamachi, V. Da Costa, S. Boukari, F. Scheurer, L. Joly, P. Ohresser, E. Otero, F. Choueikani, A. B. Gaspar, J. A. Real, W. Wulfhekel, M. Bowen, E. J. Beaurepaire, *Chemical Physics.* **2013**, *139*, 074708.

[39] S. Beniwal, X. Zhang, S. Mu, A. Naim, P. Rosa, G. Chastanet, J.-F. Létard, J. Liu, G. E. Sterbinsky, D. A. Arena, P. A. Dowben, A. Enders, *J. Phys. Condens. Matter.* **2016**, *28*, 206002.

[40] A. Pronschinske, R. C. Bruce, G. Lewis, Y. Chen, A. Calzolari, M. Buongiorno-Nardelli, D. A. Shultz, W. Youb, D. B. Dougherty, *Chem. Commun.* **2013**, *49*, 10446

[41] X. Zhang, T. Palamarciuc, J.-F. Létard, P. Rosa, E. V. Lozada, F. Torres, L. G. Rosa, B. Doudin, P. A. Dowben, *Chem. Commun.* **2014**, *50*, 2255.

[42] X. Zhang, S. Mu, G. Chastanet, N. Daro, T. Palamarciuc, P. Rosa, J.-F. Létard, J. G. Liu, E. Sterbinsky, D. A. Arena, C. Etrillard, B. Kundys, B. Doudin, P. A. Dowben, *J. Phys. Chem. C.* **2015**, *119*, 16293.

[43] J. P. Jesson, S. Trofimenko, D. R. Eaton, *J. Am. Chem. Soc.* **1967** 89:13, 3158 – 3164.

[44] V. Ksenofontov, G. Levchenko, H. Spiering, P. Gütlich, J.-F. Létard, Y. Bouhedja, O. Kahn, *Chem. Phys. Lett.* **1998**, *294*, 545.

[45] X. Zhang, T. Palamarciuc, P. Rosa, J.-F. Létard, B. Doudin, Z. Zhang, J. Wang, P. A. Dowben, *J. Phys. Chem. C.* **2012**, *116*, 23291

[46] J A. Real, M. C. Muñoz, J. Faus, X. Solans, *Inorg. Chem.* **1997**, *36*, 3008.

[47] A. L. Thompson, A. E. Goeta, J. A. Real, A. Galet, M.C. Munoz, *Chem. Commun.* **2004**, 1390.

[48] M. A. Halcrow, *Chem. Soc. Rev.* **2008**, *37*, 278.

[49] R. Bertoni, M. Cammarata, M. Lorenc, S. F. Matar, J.-F. Létard, H. T. Lemke, E. Collet, *E. Acc. Chem. Res.* **2015**, *48*, 774.

[50] M. Cammarata, R. Bertoni, M. Lorenc, H. Cailleau, S. Di Matteo, C. Mauriac, S. F. Matar, H. Lemke, M. Chollet, S. Ravy, C. Laulhé, J.-F. Létard, E. Collet, *Phys. Rev. Lett.* **2014**, *113*, 227402.

[51] N. Huse, H. Cho, K. Hong, L. Jamula, F. M. de Groot, T. K. Kim, J. K. McCuster, R. W. Schoenlein, *J. Phys. Chem. Lett.* **2011**, *2*, 880.

[52] J. K. McCusker, A. L. Rheingold, D. N. Hendrickson, *Inorg. Chem.* **1996**, *35*, 2100.

[53] W. Zhang, R. Alonso-Mori, U. Bergmann, C. Bressler, M. Chollet, A. Galler, W. Gawelda, R. G. Hadt, R. W. Hartsock, T. Kroll, K. S. Kjær, K. Kubiček, H. T. Lemke, H. W. Liang, D. A. Meyer, M. M. Nielsen, C. Purser, J. S. Robinson, E. I. Solomon, Z. Sun, D. Sokaras, T. B. van Driel, G. Vankó, T.-C. Weng, D. Zhu, K. J. Gaffney, *Nature.* **2014**, *509*, 345.

[54] P. Stock, T. Pedzinski, N. Spintig, A. Grohmann, G. Hörner, *Chem. Eur. J.* **2013**, *19*, 839.

[55] P. Stock, E. Deck, S. Hohnstein, J. Korzekwa, K. Meyer, F. W. Heinemann, F. Breher, G. Hörner, *Inorg. Chem.* **2016**, *55*, 5254.

[56] M. Hostettler, K. W. Törnroos, D. Chernyshov, B. Vangdal, H.-B. Bürgi, *Angew. Chem. Int. Ed.,.* **2004**, *43*, 4589.

[57] S. Simpson, J. Hooper, D. P. Miller, D. A. Kunkel, A. Enders, E. Zurek, *J. Phys. Chem. C* . **2016**, *120*, 6633−6641.

[58] C. Etrillard, V. Faramarzi, J.-F. Dayen, J.-F. Letard, B. Doudin, *Chem. Commun.* **2011**, *47*, 9663.

[58] F. Guillaume, Y. A. Tobon, S. Bonhommeau, J.-F. Létard, L. Moulet, E. Freysz, *Chem. Phys. Lett.* **2014**, *604*, 105.

[60] P. Braunstein, O. Siri, J. Taquet, M. Rohmer, M. Bénard, R. Welter, *A. J. Am. Chem. Soc.* **2003**, *125*, 12246.

[61] O. Siri, P. Braunstein, *Chem. Commun.* **2002** 208−209.

[62] F. Tamboura, B. C. Cazin, S. J. R. Pattacini, P. Braunstein, *Eur. J. Org. Chem.* **2009**, *20*, 3340−3350.

[63] Q. Yang, Z. O. Siri, P. Braunstein, *Chem. Commun.* **2005** 2660−2662

[64] P. Nachimuthu, J. H. Underwood, C. D. Kemp, E. M. Gullikson, D. W. Lindle, D. K. Shuh, R. C. Perera, C. In: AIP Conference Proceedings; AIP Publishing, **2004**, *05*, 454.

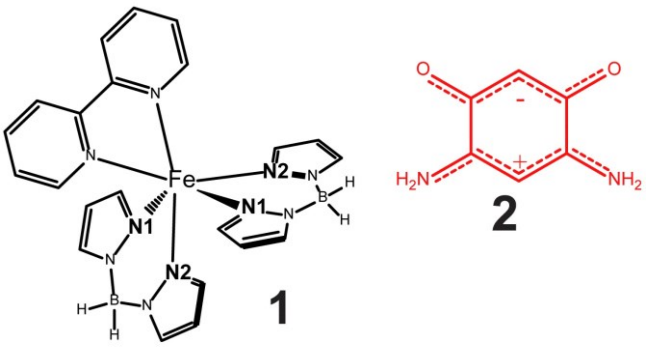

Figure 1. (a) The chemical structures of the spin crossover complex [Fe{$H_2B(pz)_2$}$_2$(bipy)] (pz = pyrazol-1-yl, bipy = 2,2'-bipyridine) (molecule **1**) and the p-benzoquinonemonoimine zwitterion, $C_6H_2(\cdots NH_2)_2(\cdots O)_2$ molecule (molecule **2**).

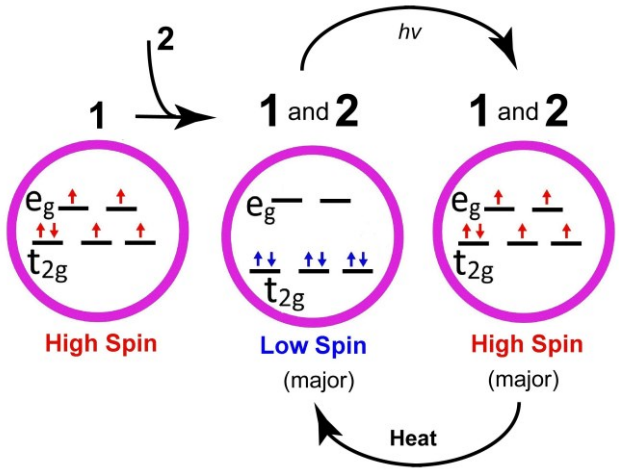

Figure 2. Schematics of the principle of reversible control of the spin state of molecule **1**, pinned in the majority LS state in the presence of molecule **2** at temperatures reaching room temperature (RT). X-ray irradiation switches the state to the majority HS state, and mild heating by an additional 10-40 K brings the molecules back into a majority LS configuration.

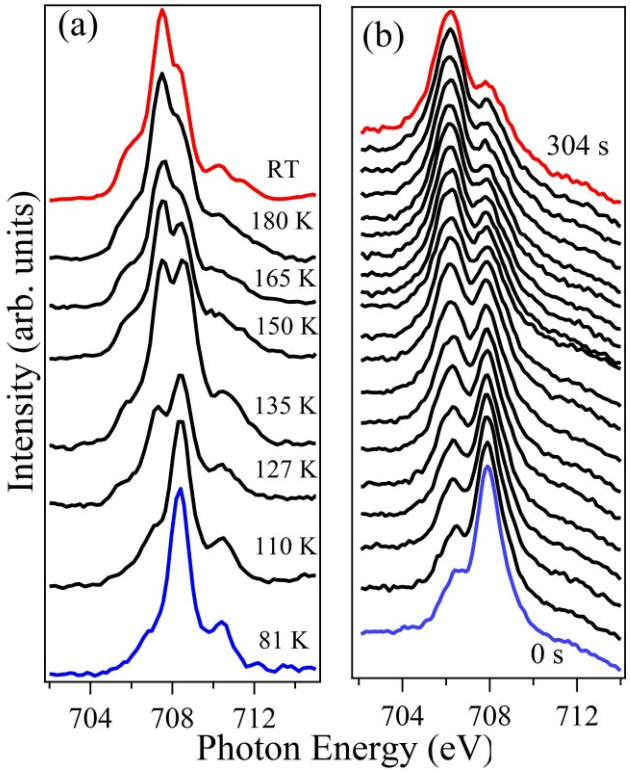

Figure 3. (a) Temperature dependent X-ray absorption spectra of molecule **1** powder; (b) Time evolution of a 5 nm thick films of molecule 1 on SiO_2 at a constant temperature of 290 K. The trapped LS state evolves into an HS state under soft X-ray exposure (with the time increasing from bottom to top) in a process analogous to SOXIESST, even though here this occurs at higher temperatures.

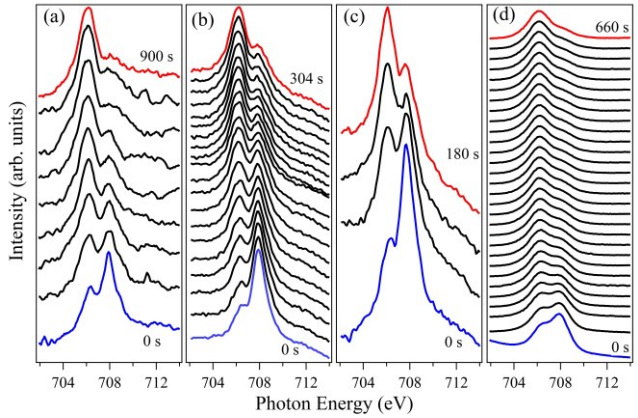

Figure 4. X-ray absorption spectra of thin films of molecule 1 on SiO_2 (a-c) and on Al_2O_3 (d), indicating time evolution of SOXIESST at (a) 200 K, (b) 290 K and (c) 345 K, for 5 nm thick films on SiO_2. Similar results are obtained for (d) 30 nm thin films on Al_2O_3, at 294 K. From bottom to top, the time is increasing and the spin state changes from the LS state (blue) to the HS state (red).

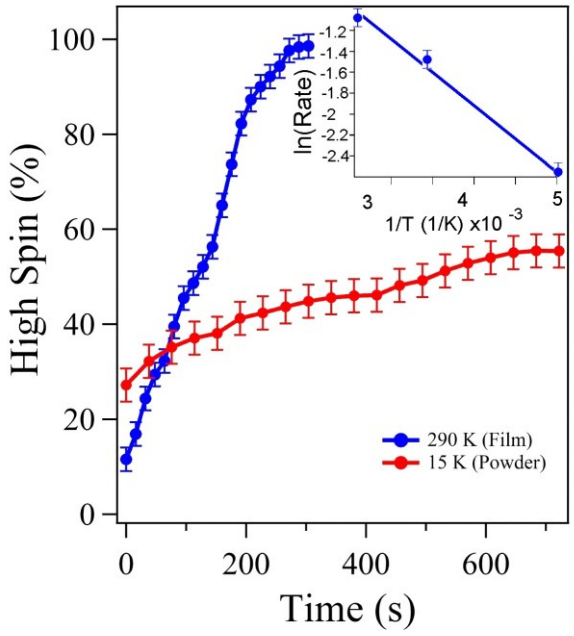

Figure 5. The evolution of the HS state fraction for 5 nm thin films of **1** on SiO_2 at 290 K (blue), and powder of **1** (red) at 15 K. The inset shows the related Arrhenius plot of the HS fraction of the thin films.

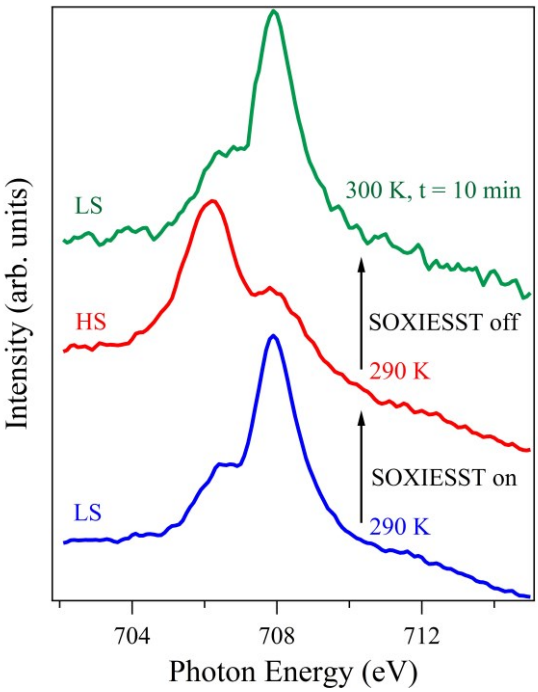

Figure 6. X-ray absorption spectra showing the 'unlocking' of 5 nm thin films of molecule **1** on SiO_2, under soft X-ray fluences (SOXIESST on), towards a HS state within about 5 min at 290 K. This is followed by a reversible return to the locked LS phase under a small increase in temperature to 300 K, within about 10 minutes.

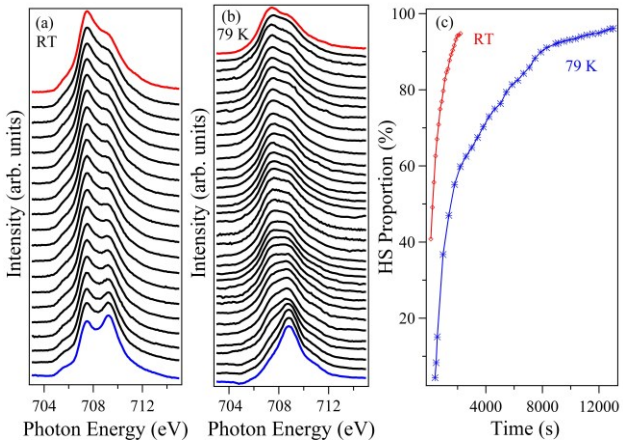

Figure 7. The evolution of high spin state occupancy for mixtures of molecules **1** and **2** in the ratio of **1**:**2**. The soft X-ray absorption at (a) RT and (b) 79 K is plotted, with increasing time from bottom to top. (c) The HS fraction evolution with time, estimated from the X-ray absorption empty t_{2g} / empty e_g ratio at 300 K (red) and 79 K (blue).

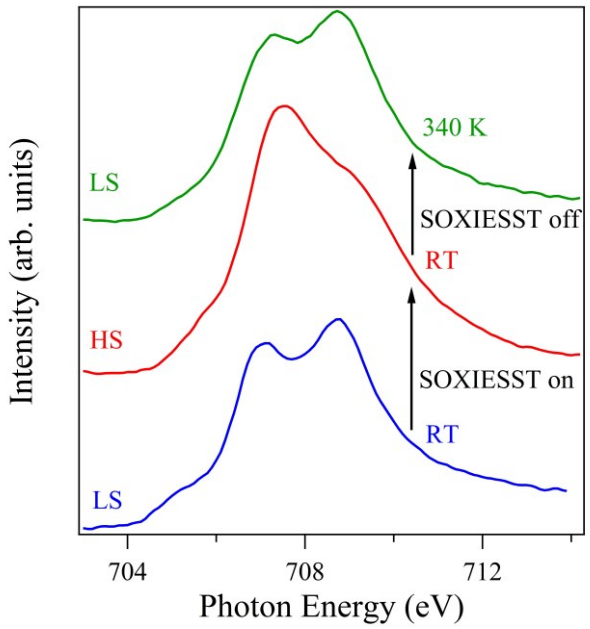

Figure 8. The locking and unlocking of the HS state occupancy for a mixture of **1** with **2** in the molar ratio of 1:2. The soft X-ray fluences switch the molecule to a stable HS state within about 5 min at 300 K. Reversibility occurs when increasing the temperature to 340 K, within about 10 min. This is schematically illustrated in Figure 2.

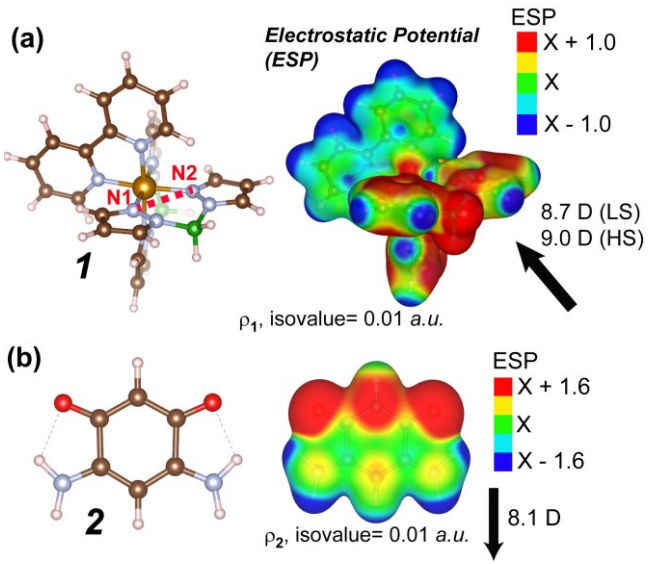

Figure 9. (a) and (b) show the ball-and-stick representations of **1** and **2** (left) alongside the computed electrostatic potential (ESP) around them (right). The ESP is coloring an isosurface (isovalue = 0.01 a.u.) of the total electron density, ρ, from each fragment; X is the median of the ESP values that are sampled on each ρ isosurface, and regions that are electron-rich/electron-poor are colored red/blue, respectively. In (a), the N1-N2 distance provides a simple metric that helps distinguish between the low-spin and high-spin electronic states. The computed electrostatic potential (ESP) around **1** is shown for the low-spin state. In (a) and (b), the computed dipole moment is shown in the bottom right, and the C atoms are colored dark brown, N atoms in blue, B atoms in green, Fe atoms in light brown and H atoms are white.

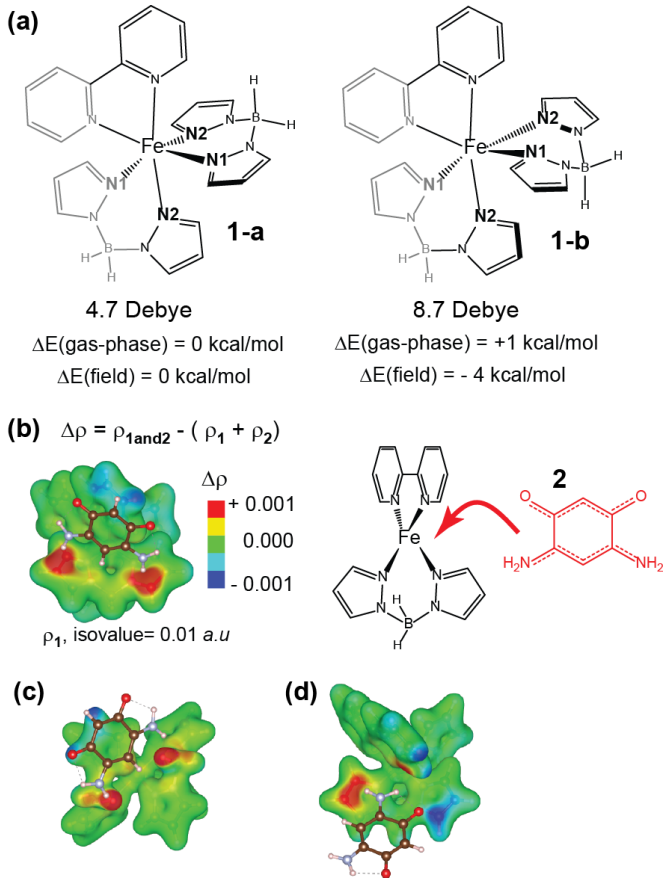

Figure 10. (a) A sketch of two energetically competitive isomers of molecule 1; the BH_2 group is closest to the adjacent bipyridine ligand in the **1-a** geometry, whereas it is instead closest to the adjacent pyrazol-1-yl ligand in the **1-b** geometry. The computed molecular dipole moment in the low-spin electronic state is shown below each molecule. Also shown are the molecules' relative electronic energies in the gas-phase and when modeled in a 2.57×10^9 $V*m^{-1}$ electric dipole field that runs parallel to their dipole moments. (b) The charge density difference ($\Delta\rho$) surrounding molecule **1**, in the **1-b** geometry, as a molecule of **2** is adsorbed, via non-covalent interactions, in the lowest-energy binding site that was considered. $\Delta\rho$ is coloring an isosurface of the total electron density, □, from molecule **1**; regions that are colored red correspond with an accumulation of electron density,

relative to the isolated fragments, and regions that are colored blue correspond with a loss of electron density. The structure around the **2** binding site is sketched to the right. (c) and (d) show how $\Delta\rho$ changes with different binding geometries of **2** to **1**; (c) shows a geometry where the N-H groups from **2** are in close contact with the B-H groups from **1**, and (d) shows a geometry that is similar to (b), but **2** is rotated to introduce an O…($H_2B(pz)_2$) interaction.

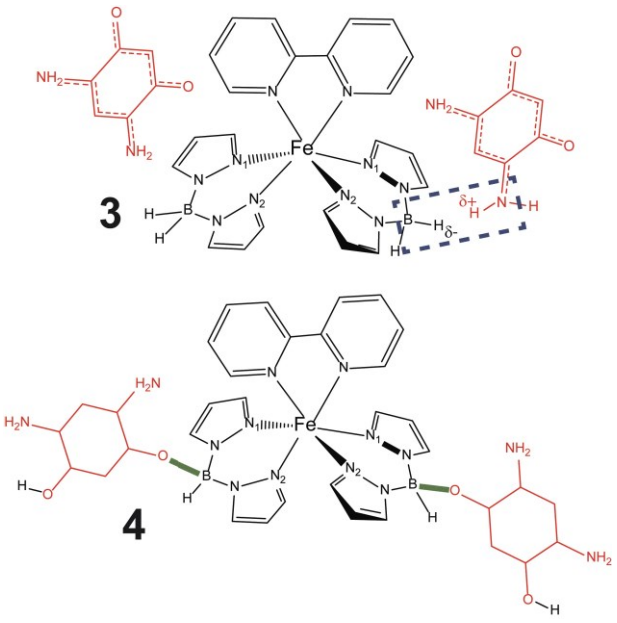

Figure 11. The chemical structures of the two structural models we considered for two molecules of **2** (red) binding to molecule **1** (black); the **2** fragments are colored red, and the 1 fragment is colored black. Model **3** corresponds with two molecules of **2** binding to **1** without forming additional covalent inter-fragment bonds. Model **4** corresponds to a possible product of a reaction between **2** and **1** that would generate a covalent B-O bond between the **1** and **2** constituents; the B-O bond is colored green. Model **4** is computed to be more stable than model **3**. In the absence of definitive evidence

of the presence or absence aromaticity of the zwitterion moieties in **4**, no double nor aromatic bonds are indicated on these moieties.

The table of contents entry:

Locking of the spin state of a molecular spin crossover system has been achieved, and room temperature optical isothermal switching from a low spin to high spin state demonstrated. Key ingredients, necessary for molecular magneto-electric, are realized and a room temperature molecular magneto-electric may now be realizable.

Keyword

Spin crossover transition, X-ray excited spin states, spin state locking, substrate interactions, zwitterion complexes.

Xin Zhang, Paulo S. Costa, James Hooper,* Daniel P. Miller, Alpha T. N'Diaye,* Sumit Beniwal, Xuanyuan Jiang, Yuewei Yin, Patrick Rosa, Lucie Routaboul,* Mathieu Gonidec, Lorenzo Poggini, Pierre Braunstein,* Bernard Doudin,* Xiaoshan Xu,* Axel Enders,* Eva Zurek,* Peter A. Dowben*

Locking and Unlocking the Molecular Spin Cross-Over Transition

ToC figure

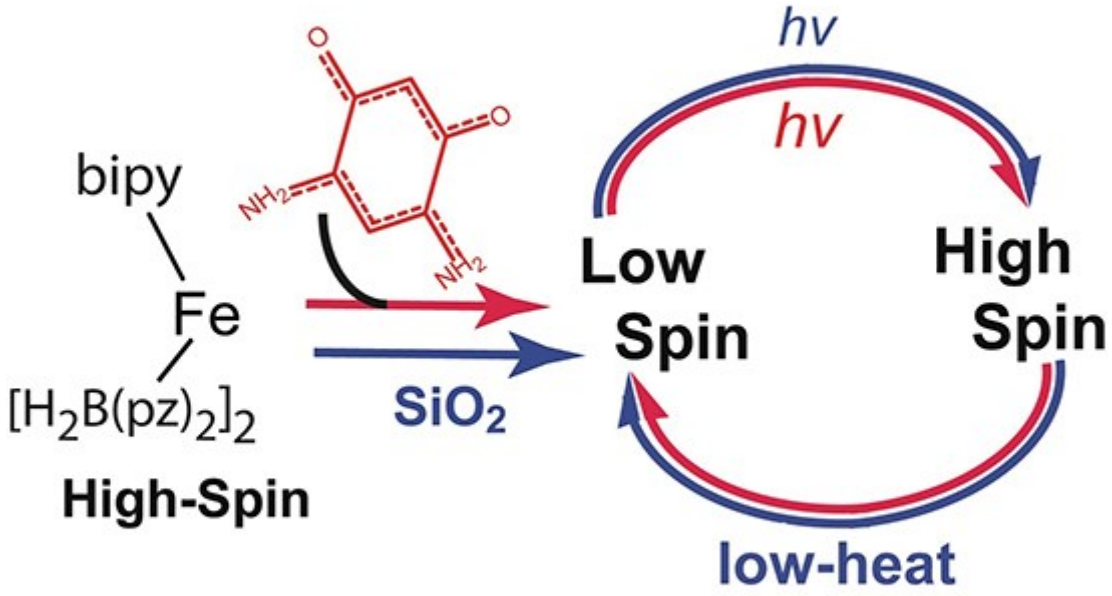

(Supporting Information can be included here using this template)

Supporting Information

Locking and Unlocking the Molecular Spin Cross-Over Transition

Xin Zhang, Paulo S. Costa, James Hooper, Daniel P. Miller, Alpha T. N'Diaye, Sumit Beniwal, Xuanyuan Jiang, Yuewei Yin, Patrick Rosa, Lucie Routaboul,* Mathieu Gonidec, Lorenzo Poggini, Pierre Braunstein,* Bernard Doudin,* Xiaoshan Xu,* Axel Enders,* Eva Zurek,* Peter A. Dowben**

Computational Details

All of the reported theory efforts on models of gas-phase 1- and/or 2 based complexes use first-principles Density Functional Theory (DFT),[1] consistent with prior efforts on 1 [2,3,4] and 2.[5-15] In this work, we use DFT as it is implemented in the Gaussian09 computational package.[16] We used the generalized gradient approximation (GGA) functional of Perdew, Burke, Ernzerhof (PBE) [16,17] in tandem with the 3rd-generation Grimme set of empirical dispersion corrections [18] (PBE+D3). All of the energetic and electronic trends that we discuss in the main text were checked with the hybrid B3LYP functional [Stephens 94] and

the meta-GGA TPSS functional [19] to ensure quantitative agreement, and the results from all three functionals (PBE+D3, B3LYP+D3, and TPSS+D3) are shown in the SI. We note that, as expected, the relative energies of the low-spin S = 0 (LS) and high-spin S = 2 (HS) states are quite sensitive to the methodology that was used (PBE+D3 and TPSS+D3 heavily favor the LS state and B3LYP+D3 favors the HS state at T= 0 K).

The Gaussian09 calculations were run with the all-electron TZVP basis set. The binding energies, $\Box G_{bind}$, of 2 to 1, are computed as $n^*\Box G_{bind}(1 \text{ and } 2) = G_{1 \text{and } 2} - (G_1 + n^*G_2)$, where G_X is the computed Gibb's free energy of compound X at a given temperature. In the discussion below, the molecule **1** model is an isolated spin crossover complex, and the **3** and **4** models (defined in the discussion below) are combinations of **1** with two molecules of **2**. The basis set superposition errors (BSSE), to correct the binding energies, were computed using the Counterpoise method [20] for the **3** model and found to be 1.5 kcal/mol for the two spin states. The binding energies that we discuss in the main text do not include this BSSE correction.

The geometric differences between the LS and HS states are consistent: the Fe-N distances are longer in the HS state, illustrating the spin crossover transition is accompanied by a structural change.[3,21,22] For example, calculations find that the distance between the coordinating N atoms in the $H_2B(pz)_2$ pyrazol-1-yl ligand of molecule **1** (labeled N1···N2, in Figure 3) is roughly 0.2 Å longer in the HS state to be compared to the 0.15 Å change found in crystal structures.[22] We have found that changes, either shortenings or lengthenings, in the N1···N2 distances correlate with changes in the Fe···N distances whenever they are mentioned in the discussion below. With regards to the interactions of molecule **1** with dipole electric

fields as discussed below, it is also worth noting the differences between the electron density distributions of the LS and HS states; as an example, the differences in the partial atomic charges of Fe in a number of different models are shown in the SI.

[1] W. Kohn, L. J. Sham, *Phys. Rev.* **1965**, *140*, A1133.

[2] E. Ludwig, H. Naggert, M. Kalläne, S. Rohlf, E. Kröger, A. Bannwarth, A. Quer, K. Rossnagel, L. Kipp, F. Tuczek, *Angew. Chem. Int. Ed.* **2014**, *53*, 3019.

[3] X. Zhang, S. Mu, G. Chastanet, N. Daro, T. Palamarciuc, P. Rosa, J.-F. Létard, J. G. Liu, E. Sterbinsky, D. A. Arena, C. Etrillard, B. Kundys, B. Doudin, P. A. Dowben, *J. Phys. Chem. C.* **2015**, *119*, 16293.

[4] X. Zhang, T. Palamarciuc, P. Rosa, J.-F. Létard, B. Doudin, Z. Zhang, J. Wang, P. A. Dowben, *J. Phys. Chem. C.* **2012**, *116*, 23291

[5] D. Delaere, P.-C. Nam, M. T. Nguyen, *Chem. Phys. Lett.* **2003**, *382*, 349.

[6] T. Höltzl, T. Veszprémi, M. T. Nguyen, *J. Phys. Org. Chem.* **2005**, *18*, 1123.

[7] L. Kong, L. Routaboul, P. Braunstein, H.-G. Park, J. Choi, J. P. Colón Córdova, E. Vega, L. G. Rosa,; B Doudin, P. Dowben, *A. RSC Advances.* **2013**, *3*, 10956 - 10961

[8] D. Kunkel, S. Simpson, J. Nitz, G. Rojas, E. Zurek, L. Routa-boul, B. Doudin, P. Braunstein, P. Dowben, A. Enders, *Chem. Comm.* **2012**, *48*, 7143 - 7145.

[9] D. Kunkel, A. J. Hooper, S. Simpson, D. Miller, L. Routaboul, P. Braunstein, B. Doudin, P. Dowben, R. Skomski, E. Zurek, A. Enders, *J. Chem. Phys.* **2015**, *142*, 101921.

[10] H. Le, T. P. C. Nam, L. V. Dao, T. Veszprémi, M. T. Nguyen, *Mol. Physics,.* **2003**, *101*, 2347.

[11] L. Rosa, G. J. Velev, Z. Zhang, J. Alvira, O. Vega, G. Diaz, L. Routaboul, P. Braunstein, B. Doudin, Y. B. Losovyj, P. A. Dowben, *Physica Status Solidi B.* **2012**, *249*, 1571.

[12] L. Routaboul, P. Braunstein, J. Xiao, Z. Zhang, P. A. Dowben, G. Dalmas, V. DaCosta, O. Félix, G. Decher, L. G. Rosa, B. Doudin, *J. Am. Chem. Soc.* **2012**, *134*, 8494−8506

[13] A. Sawicka, P. Skurski, J. Simons, *Chem. Phys. Lett.,.* **2002**, *362*, 527.

[14] S. Simpson, D. A. Kunkel, J. Hooper, J. Nitz, P. A. Dowben, L. Routaboul, P. Braunstein, B. Doudin, A. Enders, E. Zurek, *J. Phys. Chem. C* . **2013**, *117*, 16406−16415.

[15] J. Xiao, Z. Zhang, D. Wu, L. Routaboul, P. Braunstein, B. Doudin, L. G. Losovyj, Ya. B. O. Kizilkaya,; Rosa, C. N. Borca, A. Gruverman, P.A. Dowben, *Physical Chemistry Chemical Physics.* **2010**, *12*, 10329 - 10340.

[16] M. Gaussian 09, Revision E.01, Frisch, J. G. W. Trucks, H. B. Schlegel, G. E. Scuseria, M. A. Robb, J. R. Cheeseman, G. Scalmani, V. Barone, B. Mennucci, G. A. Petersson, H. Na-katsuji, M. Caricato, X. Li, H. P. Hratchian, A. F. Izmaylov, J. Bloino, G. Zheng, J. L. Sonnenberg, M. Hada, M. Ehara, K. Toyota, R. Fukuda, J. Hasegawa, M. Ishida, T. Nakajima, Y. Honda, O. Kitao, H. Nakai, T. Vreven, J. A. Montgomery Jr., J. E. Peralta, F. Ogliaro, M. Bearpark, J. J. Heyd, E. Brothers, K. N. Kudin, V. N. Staroverov, R. Kobayashi, J. Normand, K. Raghavachari, A. Rendell, J. C. Burant, S. S. Iyengar, J. Tomasi, M. Cossi, N. Rega, J. M. Millam, M. Klene, J. E. Knox, J. B. Cross, V. Bakken, C. Adamo, J.

Jaramillo, R. Gom-perts, R. E. Stratmann, O. Yazyev, A. J. Austin, R. Cammi, C. Pomelli, J. W. Ochterski, R. L. Martin, K. Morokuma, V. G. Zakrzewski, G. A. Voth, P. Salvador, J. J. Dannenberg, S. Dapprich, A. D. Daniels, Ö. Farkas, J. B. Foresman, J. V. Ortiz, J. Cioslowski, D. J. Fox, Gaussian, Inc., Wallingford CT, **2009**.

[17] J. P. Perdew, K. Burke, M. Ernzerhof, *Phys. Rev. Lett.* **1996**, *77*, 3865.

[18] S. J. Grimme, Antony, S. Ehrlich, H. J. Krieg, *Chem. Phys.* **2010**, *132*, 154104.

[19] J. Tao, J. P. Perdew, V. N. Staroverov, G. E. Scuseria, *Phys. Rev. Lett.* **2003**, *91*, 146401.

[20] F. Boys, S, F. Bernardi, *Mol. Phys.* **1970**, *19*, 553.

[21] J. Real, A. M. C. Muñoz, J. Faus, X. Solans, *Inorg. Chem.* **1997**, *36*, 3008.

[22] A. Thompson, L. A. E. Goeta, J. A. Real, A. Galet, M. C. Munoz, *Chem. Commun.* **2004**, 1390.

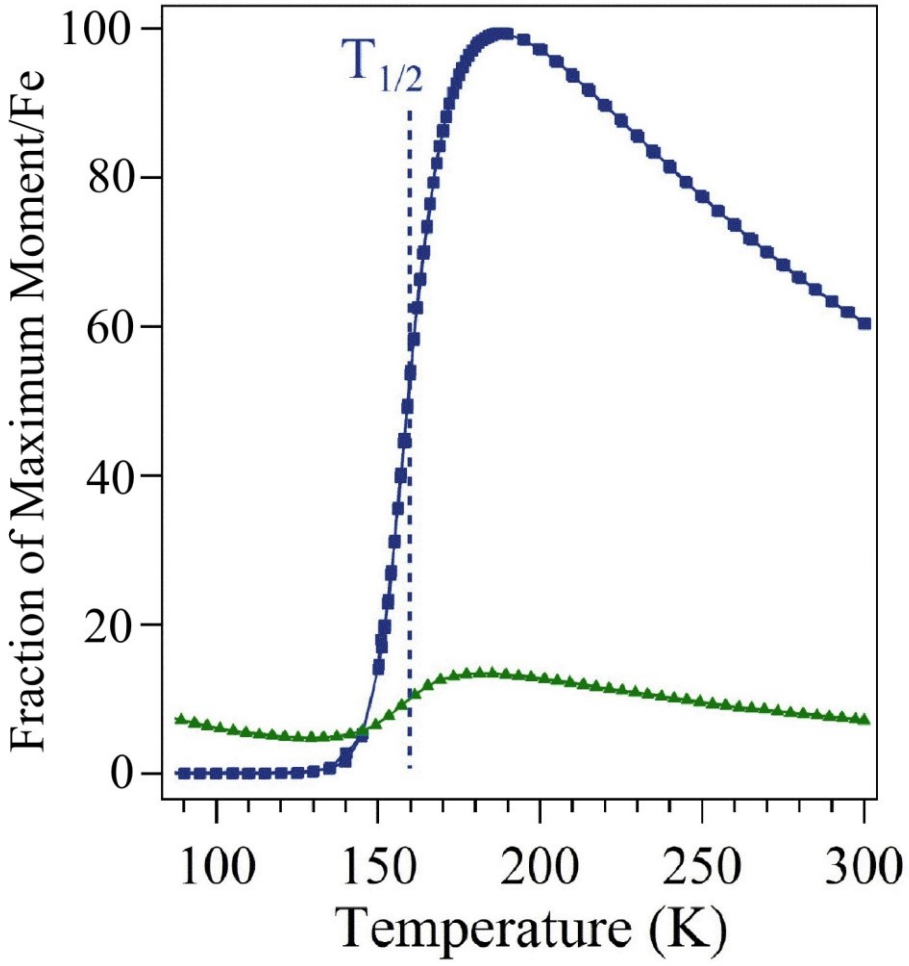

Figure S1. The suppression of the magnetic moment/Fe for the $[Fe(H_2B(pz)_2)_2(bipy)]$, i.e. molecule **1** (blue, with no additive), when the zwitterionic p-benzoquinonemonoimine $C_6H_2(\cdots NH_2)_2(\cdots O)_2$, i.e. molecule **2** is added (green). Suppression of the high spin state and the spin crossover transition is evident.

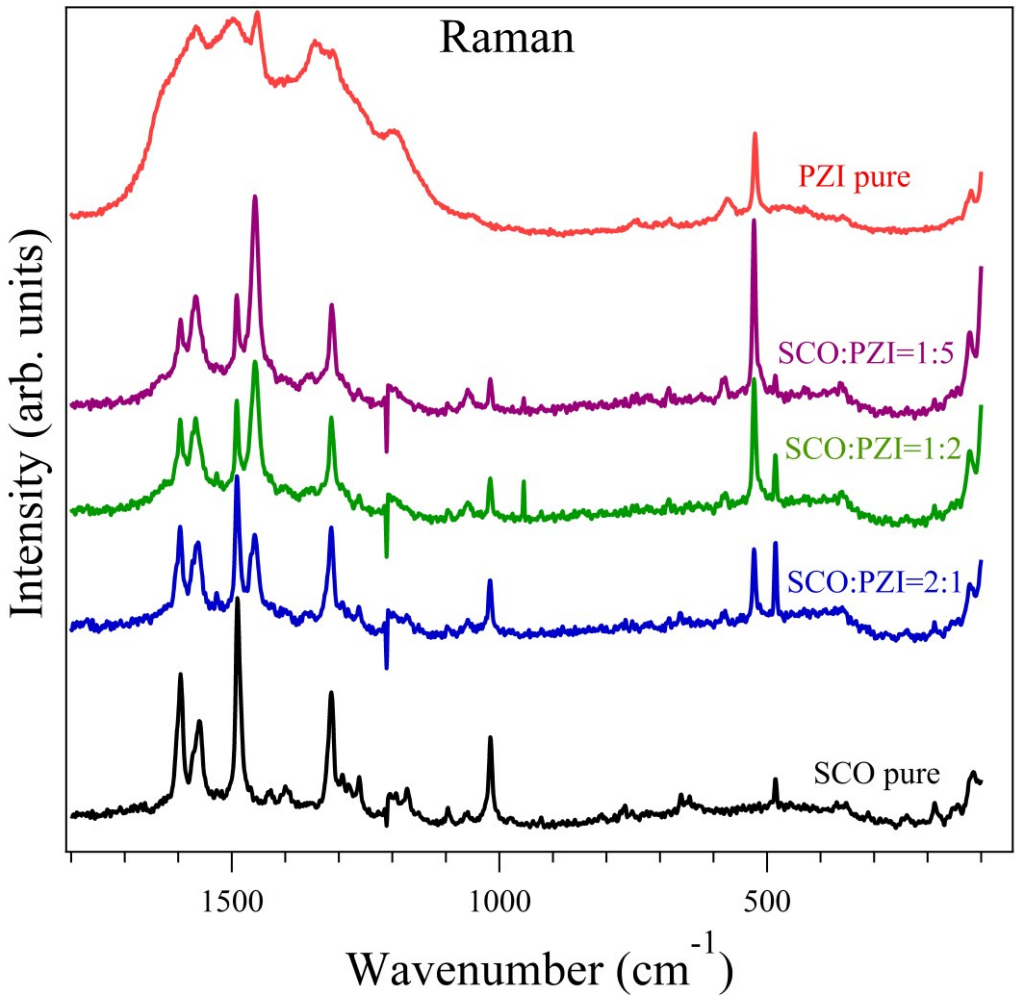

Figure S2. The experimental Raman spectra of the spin-crossover molecule $[Fe(H_2B(pz)_2)_2(bipy)]$, i.e. molecule **1** (labelled SCO in the plot above), with the zwitterionic p-benzoquinonemonoimine $C_6H_2(\cdots NH_2)_2(\cdots O)_2$, i.e. molecule **2** (labelled PZI in the plot above), fabricated using isopropyl alcohol with different ratios of **1** (SCO) *versus* **2** (PZI) (color), and without the zwitterionic p-benzoquinonemonoimine molecule (black). Of particular note is the appearance of a new peak in the 1:2 SCO:PZI spectrum at 954 cm^{-1}.

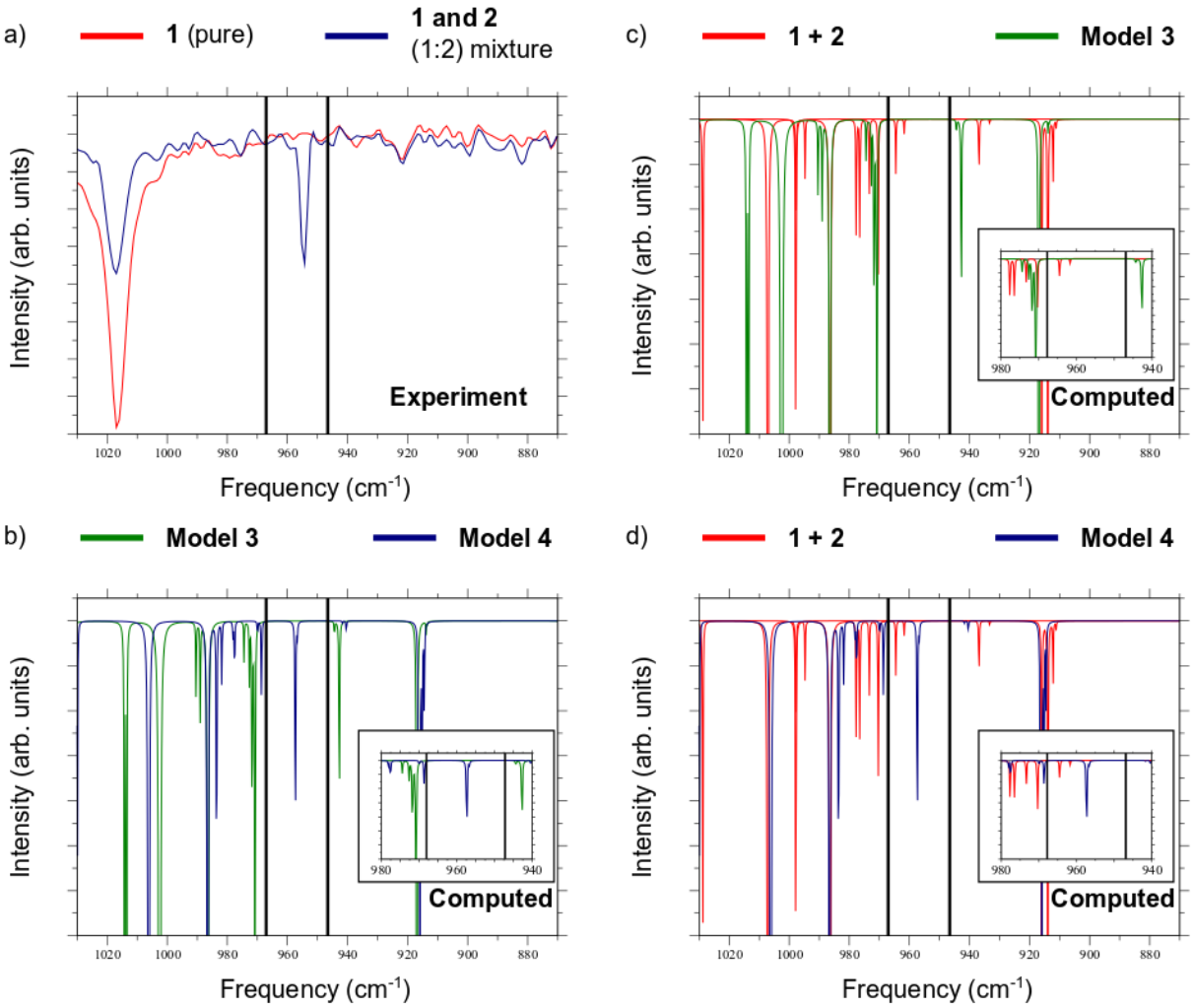

Figure S3. (a) A comparison of the experimentally measured Raman spectra of **1** (red) vs. a 1:2 mixture of molecule **1** and molecule **2** (blue) between 870 cm^{-1} and 1035 cm^{-1}. Comparison of the DFT computed Raman spectra are shown of (b) the gas-phase Model **3** complex (blue) *versus* the **1** and **2** molecules (red, the spectrum of each molecule is plotted separately), (c) the gas-phase Model **4** complex (blue) *versus* the gas-phase Model **3** complex (green), and (d) the gas-phase Model **4** complex (blue) *versus* the **1** and **2** molecules (red, the spectrum of each molecule is plotted separately). Model **4** possesses intermolecular B-O bonds, which are stretched by the mode that appears in the computed spectrum of **4** at 957 cm^{-1}. In all subfigures the black vertical lines are a guide to the eye that help highlight the mode at 957 cm^{-1}.

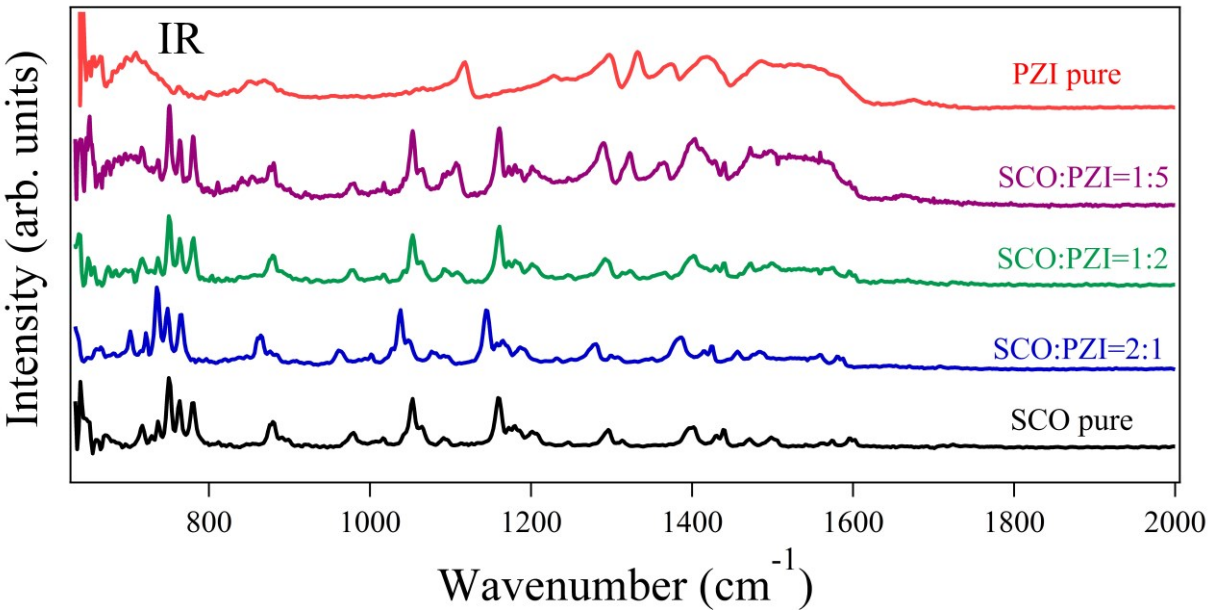

Figure S4 The experimental infra-red spectra of the spin-crossover molecule $[Fe(H_2B(pz)_2)_2(bipy)]$, i.e. molecule **1** (labelled SCO in the plot above), with the zwitterionic p-benzoquinonemonoimine $C_6H_2(\cdots NH_2)_2(\cdots O)_2$, i.e. molecule **2** (labelled PZI in the plot above), fabricated using isopropyl alcohol with different ratios of SCO vs. PZI (color), and without the zwitterionic *p*-benzoquinonemonoimine molecule (black). The IR spectra of the mixed SCO:PZI systems agree well with superimposed plots of the pure SCO and PZI spectra.

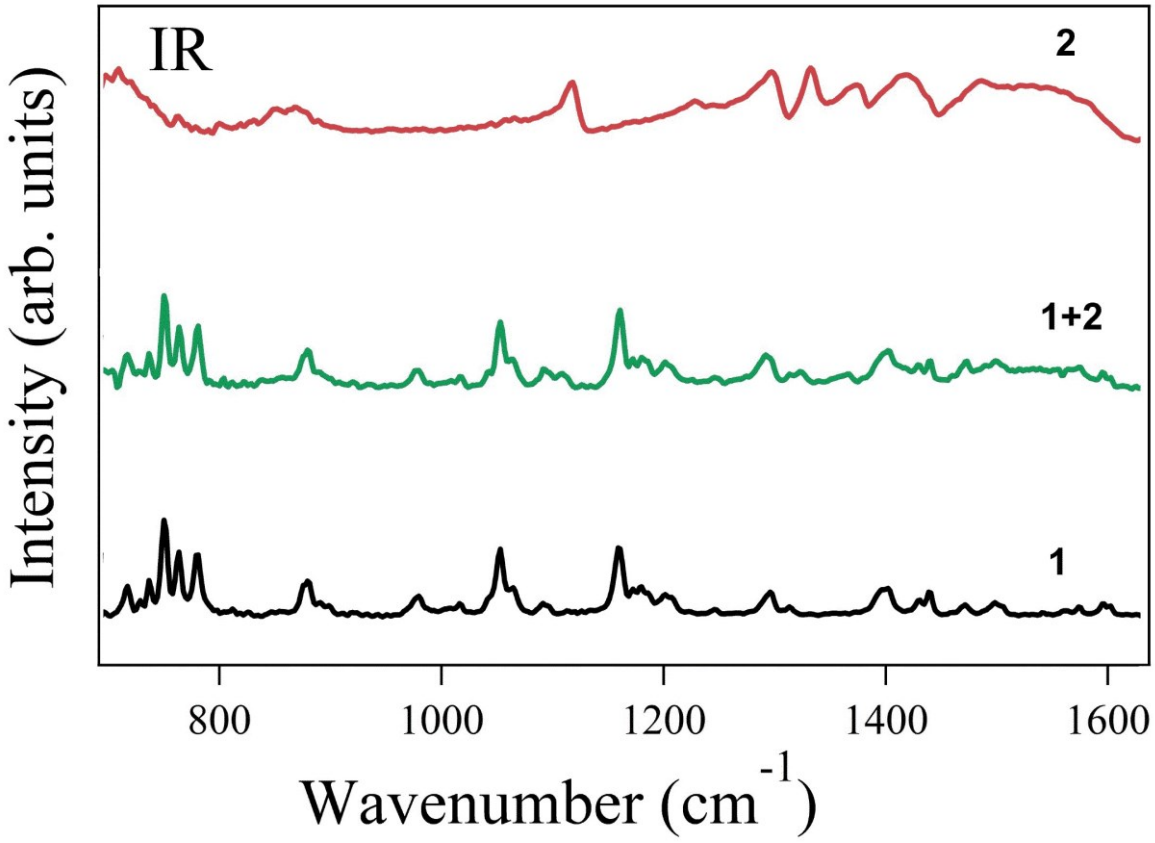

Figure S5. The measured infra-red spectra of $[Fe(H_2B(pz)_2)_2(bipy)]$, i.e. molecule **1** (the SCO - spin crossover molecule), with the zwitterionic p-benzoquinonemonoimine $C_6H_2(\cdots NH_2)_2(\cdots O)_2$, i.e. molecule **2**.

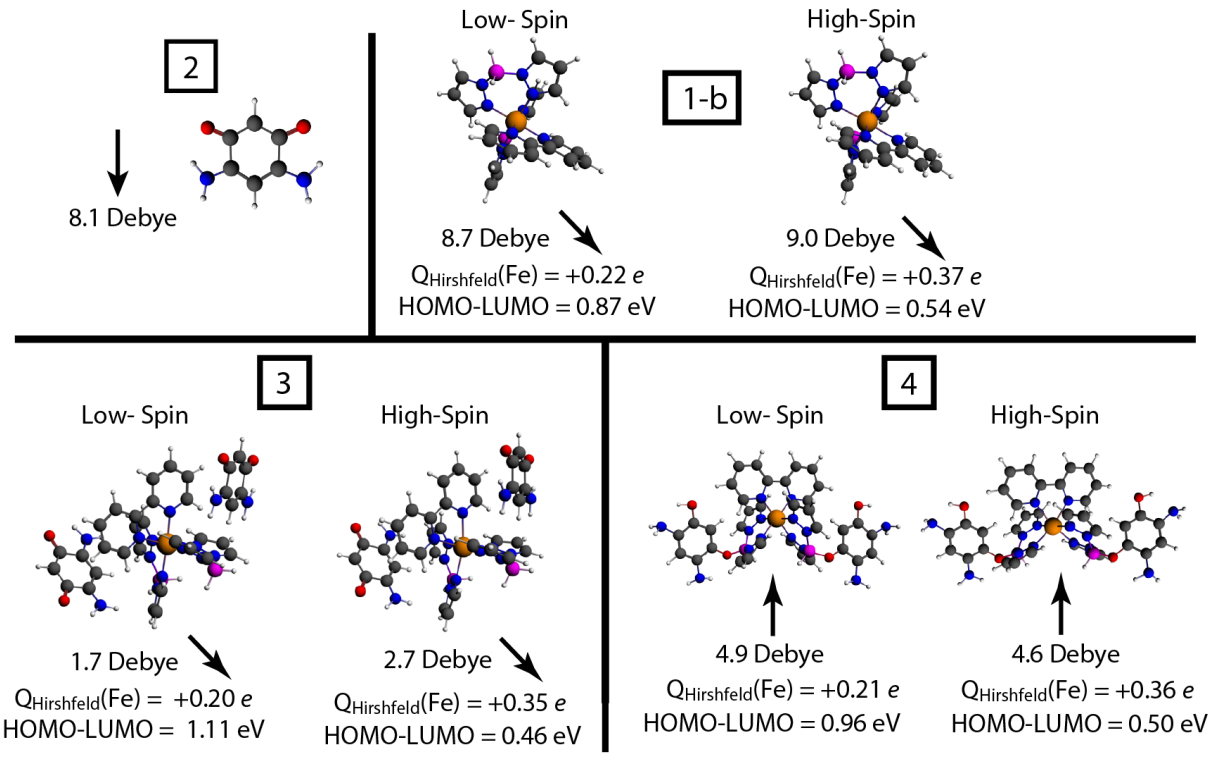

Figure S6. Computed electronic properties of the **1** (**1-b** geometry), **2**, **3**, and **4** models, including both the low-spin and high-spin states where appropriate. Shown are: 1) the computed dipole moment of each molecule, in units of Debye, 2) the computed Hirshfeld atomic charges on the Fe atom, shown as $Q_{Hirshfeld}$(Fe) in units of *e*, and 3) the difference in energy between the highest occupied molecular orbital (HOMO) and the lowest unoccupied molecular orbital (LUMO), shown as HOMO-LUMO in units of eV. All of these values were computed with the PBE+D3 functional.

	PBE+D3	B3LYP+D3	TPSS+D3
T = 0K			
$\Delta G_{T=0K}$ (**1-a, LS**)	0.0	0.0	0.0
$\Delta G_{T=0K}$ (**1-a, HS**)	+19.2	-3.6	+21.2
$\Delta G_{T=0K}$ (**1-b, LS**)	+1.1	+2.8	+1.5
$\Delta G_{T=0K}$ (**1-b, HS**)	+20.4	-1.9	+22.4
T = 298 K			
$\Delta G_{T=298K}$ (**1-a, LS**)	0.0	0.0	0.0
$\Delta G_{T=298K}$ (**1-a, HS**)	+14.6	-7.3	+18.3
$\Delta G_{T=298K}$ (**1-b, LS**)	+1.2	+3.0	+1.8
$\Delta G_{T=298K}$ (**1-b, HS**)	+15.5	-6.6	+16.6

Table S1: Relative computed Gibb's free energies, ΔG, between the **1-a** and **1-b** geometries in their lowest-energy low-spin (LS) and high-spin (HS) electronic configurations at T = 0 K (top) and T = 298 K (bottom), expressed in kcal/mol. The scale of ΔG is set to reference the LS electronic configuration of the **1-a** geometry at each temperature. The two trends we wish to stress are: 1) the **1-b** geometry is generally 1-3 kcal/mol less stable than the **1-a** geometry, and 2) the difference in energy between the LS and HS electronic states is consistently decreased, in favor of the HS state, at T = 298 K vs. the computed difference at T = 0 K.

	PBE+D3	B3LYP+D3	TPSS+D3
$\Delta G_{T=0K}$ (**3, LS**)	-16.5	-16.0	-16.3
$\Delta G_{T=0K}$ (**4, LS**)	-36.6	-40.3	-36.1
$\Delta G_{T=298K}$ (**3, LS**)	-7.3	-0.7	-4.3
$\Delta G_{T=298K}$ (**4, LS**)	-23.6	-22.9	-22.1

Table S2: The binding energies, ΔG_{bind}, of **2** to **1** to form the **3** and **4** geometries at T=0K or T=298K when **1** is in its low-spin state in the 1-b geometry, expressed in kcal/mol. ΔG_{bind} is computed as $\Delta G_{bind}(\mathbf{X}) = 0.5^* [\Delta G_{\mathbf{X}} - (\Delta G_{\mathbf{1}} + 2^*\Delta G_{\mathbf{2}})]$, where ΔG_X is the computed free energy of **3** or **4**, and $\Delta G_{\mathbf{1}}$ / $\Delta G_{\mathbf{2}}$ are the computed free energies of the respective optimized **1** / **2** geometries. The model **3** structure (shown in Figure 10 of the main text) is a low-energy structure of two **2** molecules binding to **1-b** without forming any new covalent bonding interactions, and the **4** structure (also shown in Figure 10 of the main text) is a model of what could result from a hydroboration reaction between **1** and **2**. Note that ΔG(**4**) is consistently much lower than ΔG(**3**). Also note that the HS electronic state is computed to have lower (ie. more stable and more negative) binding energies in both models **3** and **4** with the B3LYP+D3 functional, but they are not shown in the above table.

Molecular Geometries

1-a geometry -- optimized with the PBE+D3 functional, XYZ format

59

N	1.378329	-0.970573	-0.825410
N	1.378783	0.967847	0.827150
C	2.636079	0.551142	0.475645
C	3.783401	1.142521	1.015096
C	3.658273	2.174991	1.939025
C	2.373052	2.583655	2.309829
C	1.269672	1.963012	1.738527
C	1.268684	-1.965823	-1.736555
C	2.371761	-2.587592	-2.307276
C	3.657163	-2.179869	-1.936095
C	3.782828	-1.147281	-1.012360
C	2.635798	-0.554821	-0.473454
H	0.253835	-2.245346	-2.006369
H	2.214914	-3.387650	-3.030684
H	4.541768	-2.652734	-2.363788
H	4.768274	-0.793786	-0.709994
H	4.768652	0.788268	0.712977
H	4.543100	2.647062	2.367126
H	2.216599	3.383715	3.033322
H	0.254966	2.243477	2.007906
N	-0.091297	-1.233461	1.577210
N	-0.645037	-2.478623	1.589565
N	-1.900762	-2.305172	-0.582152

N	-1.530821	-1.026885	-0.888909
B	-1.050017	-3.251175	0.305072
C	-0.623786	-2.974872	2.848168
C	-0.040759	-2.031769	3.689206
C	0.271366	-0.956676	2.849535
C	-2.479160	-0.531603	-1.714815
C	-3.456884	-1.502251	-1.964110
C	-3.054845	-2.609089	-1.222874
H	0.125269	-2.106361	4.758155
H	-1.018561	-3.966417	3.042722
H	-3.498185	-3.591283	-1.097525
H	-4.340141	-1.405651	-2.585697
H	-0.046795	-3.618116	-0.279522
H	-1.743510	-4.192264	0.630487
H	0.711205	-0.000321	3.104231
H	-2.417289	0.491991	-2.065685
N	-0.086881	1.233096	-1.577037
N	-0.638429	2.479245	-1.590051
N	-1.896712	2.308516	0.580341
N	-1.529926	1.029303	0.887171
B	-1.043132	3.252731	-0.306039
C	-0.615008	2.975342	-2.848669
C	-0.032792	2.031144	-3.689045
C	0.276551	0.955554	-2.848978

C -3.050751 2.614858 1.219935

C -3.456040 1.508735 1.960506

C -2.480252 0.535983 1.712003

H 0.134410 2.105322 -4.757839

H -1.007804 3.967575 -3.043722

H -3.491742 3.598074 1.094305

H -4.340132 1.413940 2.581187

H -0.039776 3.617745 0.279572

H -1.734334 4.195242 -0.632229

H 0.714881 -0.001638 -3.103151

H -2.421063 -0.487812 2.062753

Fe -0.073447 -0.000215 0.000064

1-b geometry -- optimized with the PBE+D3 functional, XYZ format

59

N 1.362619 1.006238 0.780525

N 1.362618 -1.006238 -0.780524

C 2.621764 -0.598546 -0.415236

C 3.767380 -1.305467 -0.796569

C 3.643016 -2.461024 -1.560398

C 2.357047 -2.890459 -1.905677

C 1.254756 -2.150954 -1.498159

C	1.254758	2.150954	1.498159
C	2.357049	2.890457	1.905678
C	3.643018	2.461022	1.560398
C	3.767381	1.305465	0.796568
C	2.621764	0.598545	0.415236
H	0.242160	2.459399	1.746378
H	2.199418	3.800230	2.485211
H	4.525467	3.024866	1.864181
H	4.749585	0.953583	0.481247
H	4.749585	-0.953585	-0.481248
H	4.525465	-3.024868	-1.864181
H	2.199415	-3.800231	-2.485210
H	0.242158	-2.459399	-1.746377
N	-1.452387	0.988908	1.049565
N	-2.330557	1.892586	0.539960
N	-1.174978	2.207175	-1.673920
N	-0.130727	1.370308	-1.430166
B	-2.568957	2.079837	-0.982780
C	-3.023109	2.469743	1.549150
C	-2.583982	1.930487	2.756277
C	-1.595944	1.008072	2.394306
C	0.856838	1.701927	-2.291502
C	0.441562	2.757392	-3.112957
C	-0.851263	3.047746	-2.683856

H	-2.936221	2.164744	3.754694
H	-3.779530	3.214670	1.326548
H	-1.569268	3.789296	-3.017127
H	1.004529	3.245432	-3.900907
H	-3.174246	1.129348	-1.431555
H	-3.158321	3.128685	-1.148371
H	-0.989178	0.358210	3.014898
H	1.801453	1.169204	-2.277182
N	-1.452387	-0.988908	-1.049565
N	-2.330558	-1.892585	-0.539960
N	-1.174979	-2.207175	1.673920
N	-0.130728	-1.370308	1.430166
B	-2.568958	-2.079835	0.982780
C	-3.023111	-2.469741	-1.549150
C	-2.583983	-1.930486	-2.756277
C	-1.595945	-1.008071	-2.394306
C	-0.851265	-3.047746	2.683855
C	0.441561	-2.757394	3.112956
C	0.856837	-1.701928	2.291502
H	-2.936222	-2.164743	-3.754694
H	-3.779533	-3.214667	-1.326548
H	-1.569270	-3.789296	3.017127
H	1.004527	-3.245435	3.900905
H	-3.174246	-1.129345	1.431555

H -3.158323 -3.128682 1.148372

H -0.989178 -0.358210 -3.014898

H 1.801452 -1.169205 2.277183

Fe -0.101324 0.000000 0.000000

---

2 geometry -- optimized with the PBE+D3 functional, XYZ format

16

N 2.408790 1.233951 0.000104

N -2.408790 1.233949 0.000051

O 2.383863 -1.322880 -0.000133

O -2.383863 -1.322879 -0.000076

C 1.187730 0.721098 -0.000002

C 0.000000 -1.498496 0.000211

C 1.233219 -0.824069 -0.000026

C -1.187730 0.721098 -0.000009

C 0.000000 1.447861 -0.000125

C -1.233219 -0.824069 0.000011

H -0.000001 2.541639 -0.000111

H 0.000000 -2.587982 0.000175

H -3.146716 0.511214 0.000021

H -2.608857 2.227076 -0.000010

H 2.608855 2.227078 0.000047

H 3.146715 0.511216 0.000103

---

3 geometry -- optimized with the PBE+D3 functional, XYZ format

91

N 4.223001 1.499666 2.392647

N 5.350498 -1.587449 -1.109127

N -4.230045 1.495042 -2.399010

N -5.343190 -1.586611 1.112359

O 5.797984 3.243515 1.334854

O 6.996414 0.144560 -2.077528

O -5.802688 3.239489 -1.338804

O -6.987691 0.145528 2.082601

C 4.877732 1.058457 1.331322

C 6.525587 1.796110 -0.419143

C 5.802905 2.139273 0.738768

C 5.448861 -0.477574 -0.392051

C 4.735588 -0.209805 0.772247

C 6.421948 0.532896 -1.031963

C -4.880453 1.055290 -1.334396

C -6.525525 1.793647 0.418416

C -5.805257 2.136048 -0.741210

C -5.444780 -0.478227 0.393432

C	-4.734436	-0.211436	-0.772849
C	-6.417410	0.532254	1.034112
H	4.038176	-0.938986	1.191250
H	7.196197	2.535761	-0.856505
H	5.941707	-1.582211	-1.952253
H	4.663960	-2.319227	-0.930241
H	3.515466	0.955314	2.887990
H	4.451390	2.474541	2.633962
H	-4.037595	-0.940715	-1.192623
H	-7.195576	2.533383	0.856478
H	-5.932547	-1.580581	1.956798
H	-4.657219	-2.318722	0.932510
H	-3.522218	0.951123	-2.894389
H	-4.460001	2.469372	-2.641109
N	1.141929	0.980032	-0.575963
N	-1.144675	0.977104	0.579403
C	-0.667459	2.232565	0.300548
C	-1.415408	3.382780	0.574453
C	-2.665819	3.268261	1.174088
C	-3.132957	1.991702	1.492726
C	-2.357316	0.883717	1.170225
C	2.355777	0.889627	-1.164818
C	3.128874	1.999577	-1.486657
C	2.657544	3.275044	-1.169734

C	1.406124	3.386429	-0.571641
C	0.661097	2.234268	-0.297915
H	2.703295	-0.115878	-1.381560
H	4.104068	1.857276	-1.950961
H	3.260383	4.159959	-1.373961
H	1.005132	4.365220	-0.310084
H	-1.017459	4.362551	0.311910
H	-3.270919	4.151608	1.378409
H	-4.106818	1.846906	1.958991
H	-2.701800	-0.122628	1.388030
N	1.227114	-1.882516	-0.729333
N	1.909994	-2.789539	0.017998
N	1.637966	-1.587812	2.231316
N	0.929806	-0.527124	1.746596
B	1.714719	-2.988475	1.544416
C	2.651939	-3.584392	-0.793191
C	2.456600	-3.176192	-2.111931
C	1.562968	-2.103336	-2.021684
C	0.954966	0.433229	2.696814
C	1.673507	-0.015286	3.816567
C	2.090266	-1.301380	3.474948
H	2.888196	-3.602638	-3.010850
H	3.232548	-4.397194	-0.367363
H	2.670503	-2.037014	4.021978

H	1.840947	0.509193	4.751842
H	0.698545	-3.613994	1.757311
H	2.700278	-3.551042	1.977764
H	1.135862	-1.493352	-2.809642
H	0.462189	1.384910	2.533461
N	-1.224882	-1.886037	0.727667
N	-1.907363	-2.791888	-0.021451
N	-1.635910	-1.586593	-2.232799
N	-0.929781	-0.525443	-1.746130
B	-1.710952	-2.988333	-1.548003
C	-2.648733	-3.588912	0.788135
C	-2.453384	-3.183428	2.107712
C	-1.560351	-2.109872	2.019608
C	-2.087740	-1.299253	-3.476380
C	-1.672787	-0.012045	-3.815977
C	-0.955832	0.436123	-2.695084
H	-2.884531	-3.612081	3.005801
H	-3.228944	-4.401130	0.360681
H	-2.666468	-2.035053	-4.024790
H	-1.840144	0.513373	-4.750747
H	-0.693621	-3.611951	-1.761047
H	-2.695354	-3.551821	-1.982751
H	-1.133374	-1.501491	2.808869
H	-0.464811	1.388431	-2.530195

Fe -0.000057 -0.502872 0.000453

---

4 geometry -- optimized with the PBE+D3 functional, XYZ format

91

N -5.480803 -3.982267 -0.908500

N -8.082381 -0.297168 1.217926

O -3.551580 -2.239836 -1.468553

O -6.011553 1.335559 0.722451

C -5.685534 -2.635875 -0.568476

C -4.746286 -0.384569 -0.395358

C -4.632531 -1.714835 -0.811944

C -6.948083 -0.856094 0.516618

C -6.832181 -2.185816 0.094064

C -5.894330 0.038876 0.280400

H -7.645777 -2.886949 0.301768

H -3.949070 0.327772 -0.592472

H -6.909511 1.329257 1.143454

H -8.934826 -0.340101 0.655975

H -4.738760 -4.086876 -1.599422

H -6.324278 -4.488079 -1.165327

N 5.480850 -3.982256 0.908592

N 8.082108 -0.297206 -1.218310

O	3.551587	-2.239863	1.468650
O	6.011245	1.335470	-0.722802
C	5.685504	-2.635877	0.568466
C	4.746155	-0.384620	0.395267
C	4.632483	-1.714861	0.811952
C	6.947892	-0.856124	-0.516863
C	6.832081	-2.185819	-0.094195
C	5.894121	0.038820	-0.280626
H	7.645688	-2.886935	-0.301916
H	3.948925	0.327701	0.592395
H	6.909167	1.329171	-1.143883
H	8.265376	-0.789764	-2.094720
H	6.324366	-4.488018	1.165382
H	4.738868	-4.086852	1.599580
N	1.106675	2.090505	-0.631892
N	-1.106537	2.090583	0.631926
C	-0.659786	3.347119	0.311482
C	-1.441155	4.483582	0.541774
C	-2.713197	4.344704	1.090759
C	-3.173442	3.059961	1.396645
C	-2.345458	1.969078	1.163512
C	2.345591	1.968916	-1.163470
C	3.173640	3.059745	-1.396625
C	2.713464	4.344523	-1.090778

C	1.441427	4.483488	-0.541805
C	0.659992	3.347074	-0.311485
H	2.667401	0.954600	-1.388162
H	4.178706	2.878107	-1.776527
H	3.343817	5.218954	-1.255883
H	1.060013	5.466760	-0.265613
H	-1.059688	5.466826	0.265554
H	-3.343499	5.219175	1.255844
H	-4.178517	2.878396	1.776561
H	-2.667325	0.954786	1.388234
N	1.094351	-0.752790	-0.885683
N	1.887782	-1.665611	-0.260408
N	2.015955	-0.353467	1.951229
N	1.155156	0.635963	1.595853
B	2.172256	-1.765205	1.271137
C	2.426158	-2.508790	-1.177315
C	1.983937	-2.128209	-2.437638
C	1.152797	-1.026104	-2.209005
C	1.265002	1.608906	2.527567
C	2.197473	1.236064	3.504320
C	2.646870	-0.016702	3.104239
H	2.223726	-2.589565	-3.388897
H	3.097402	-3.301569	-0.863283
H	3.376613	-0.693595	3.534625

H 2.505969 1.801939 4.376306

H 8.934605 -0.340079 -0.656435

H 1.420634 -2.554607 1.803706

H 0.589501 -0.426635 -2.914446

H 0.665130 2.508974 2.453939

N -1.094358 -0.752711 0.885800

N -1.887838 -1.665506 0.260551

N -2.015930 -0.353437 -1.951131

N -1.155094 0.635971 -1.595780

B -2.172264 -1.765154 -1.271000

C -2.426277 -2.508618 1.177483

C -1.984043 -2.128020 2.437796

C -1.152833 -1.025974 2.209131

C -2.646826 -0.016685 -3.104155

C -2.197375 1.236048 -3.504275

C -1.264893 1.608885 -2.527529

H -2.223869 -2.589326 3.389069

H -3.097562 -3.301371 0.863472

H -3.376594 -0.693563 -3.534522

H -2.505843 1.801907 -4.376282

H -1.420615 -2.554568 -1.803514

H -8.265716 -0.789680 2.094348

H -0.589507 -0.426514 2.914556

H -0.664985 2.508931 -2.453929

Fe 0.000030 0.632121 0.000038

Lowest-energy geometry that we considered of **2** binding to **1-a** -- optimized with the PBE+D3 functional, XYZ format

75

N -2.867739 1.421732 -2.029615

N -3.915850 -2.811317 -0.037731

O -4.569654 2.569675 -0.441978

O -5.735512 -1.656353 1.407239

C -3.519573 0.594709 -1.225643

C -5.363030 0.509439 0.473779

C -4.560098 1.314100 -0.353589

C -4.049248 -1.508671 -0.250813

C -3.273731 -0.771091 -1.136781

C -5.151914 -0.876933 0.615647

H -2.496473 -1.243495 -1.738558

H -6.113824 0.988375 1.102419

H -4.545188 -3.182101 0.685106

H -3.132090 -3.341623 -0.409467

H -2.071818 1.120686 -2.590702

H -3.126172 2.409313 -1.913609

N	0.584026	1.810915	-0.121454
N	-0.409580	-0.209376	1.083123
C	-1.154817	0.932421	1.220397
C	-2.307697	0.970141	2.009318
C	-2.725372	-0.177819	2.674850
C	-1.960358	-1.338345	2.538141
C	-0.818127	-1.314544	1.746103
C	1.149026	2.796786	-0.856830
C	0.559242	4.043936	-1.022905
C	-0.672427	4.305452	-0.413733
C	-1.265744	3.301311	0.344583
C	-0.617021	2.069400	0.484658
H	2.097498	2.547317	-1.325779
H	1.068545	4.796656	-1.624827
H	-1.167751	5.269175	-0.536578
H	-2.248481	3.453013	0.790442
H	-2.881571	1.892131	2.089711
H	-3.638921	-0.174167	3.268744
H	-2.243423	-2.264297	3.038761
H	-0.186834	-2.192140	1.631619
N	2.162593	0.403837	1.783296
N	3.329260	1.101717	1.885541
N	3.985652	1.010612	-0.534045
N	2.921063	0.265312	-0.953069

B	3.945039	1.923628	0.721827
C	3.762745	1.080132	3.167006
C	2.859203	0.347516	3.930796
C	1.878000	-0.060065	3.020592
C	3.319725	-0.398591	-2.061327
C	4.641414	-0.062420	-2.376980
C	5.027395	0.828813	-1.380083
H	2.907245	0.131527	4.992262
H	4.678434	1.596788	3.434205
H	5.964127	1.345684	-1.200500
H	5.237272	-0.429175	-3.205408
H	3.275013	2.919507	0.523821
H	5.086685	2.206366	1.018805
H	1.003750	-0.674763	3.194517
H	2.648466	-1.092656	-2.554029
N	0.358410	-0.444970	-1.687563
N	-0.031350	-1.688795	-2.085105
N	1.243391	-2.980973	-0.349614
N	1.810112	-1.901683	0.270587
B	-0.091340	-2.911641	-1.126993
C	-0.434024	-1.656603	-3.378320
C	-0.303177	-0.352716	-3.849993
C	0.207956	0.366448	-2.759654
C	2.006840	-4.081081	-0.133114

C 3.101254 -3.715424 0.642137

C 2.942470 -2.340580 0.860312

H -0.511645 0.015233 -4.848918

H -0.776177 -2.565145 -3.862510

H 1.709478 -5.036432 -0.552527

H 3.908941 -4.350327 0.988868

H -1.037168 -2.779640 -0.366410

H -0.201756 -3.913790 -1.802428

H 0.510543 1.405773 -2.709129

H 3.583665 -1.645963 1.391011

Fe 1.231118 -0.009683 0.063579

Lowest-energy geometry that we considered of **2** binding to **1-b** -- optimized with the PBE+D3 functional, XYZ format

75

N 3.322736 1.468989 1.906443

N 3.597722 -2.715788 -0.432265

O 5.330589 2.339694 0.546218

O 5.683241 -1.852348 -1.684851

C 3.847879 0.570216 1.089913

C	5.660392	0.287461	-0.628391
C	5.041696	1.142273	0.301760
C	3.993963	-1.508861	-0.055269
C	3.369114	-0.725570	0.909823
C	5.219838	-1.030383	-0.858362
H	2.487572	-1.083588	1.446331
H	6.514938	0.658657	-1.194173
H	4.178763	-3.121885	-1.178615
H	2.730322	-3.152811	-0.120015
H	2.491364	1.302475	2.475641
H	3.806827	2.377278	1.873065
N	-1.949517	1.757049	-0.035864
N	0.275922	0.871811	-0.913343
C	0.198145	2.243109	-0.901936
C	1.256261	3.046013	-1.340694
C	2.404408	2.453923	-1.857497
C	2.451102	1.060311	-1.936620
C	1.388862	0.313050	-1.439950
C	-3.228394	2.101533	0.248918
C	-3.680808	3.413857	0.198414
C	-2.797686	4.432780	-0.173148
C	-1.496304	4.084419	-0.520620
C	-1.096480	2.745129	-0.458417
H	-3.886348	1.285438	0.536016

H	-4.719991	3.626590	0.449427
H	-3.124210	5.472250	-0.215651
H	-0.791478	4.844090	-0.857862
H	1.175568	4.131118	-1.277568
H	3.248683	3.060536	-2.184931
H	3.324329	0.548747	-2.339790
H	1.416658	-0.773369	-1.448486
N	-2.760717	-0.735024	0.995310
N	-3.714869	-1.569501	0.502515
N	-3.156604	-1.253305	-1.929386
N	-2.162748	-0.341614	-1.743934
B	-3.580245	-2.305309	-0.858139
C	-4.692669	-1.734605	1.422637
C	-4.373460	-0.983725	2.551944
C	-3.156630	-0.370359	2.236993
C	-2.010904	0.327564	-2.909113
C	-2.905284	-0.168229	-3.865291
C	-3.613992	-1.165822	-3.200234
H	-4.938189	-0.899066	3.473700
H	-5.537121	-2.378954	1.202631
H	-4.413021	-1.820658	-3.530887
H	-3.026593	0.159350	-4.891851
H	-2.750924	-3.186312	-0.772754
H	-4.674166	-2.728506	-1.169900

H	-2.550238	0.305781	2.828906
H	-1.275586	1.120105	-2.995797
N	-0.410169	-1.836849	-0.236172
N	0.013496	-2.619065	0.789897
N	0.088348	-0.777269	2.529930
N	-0.318282	0.234915	1.711417
B	-0.217433	-2.290311	2.287942
C	0.493950	-3.791234	0.302746
C	0.390145	-3.767151	-1.087487
C	-0.176060	-2.520513	-1.379375
C	0.597683	-0.261551	3.673368
C	0.527595	1.129407	3.605743
C	-0.049801	1.393116	2.352989
H	0.668054	-4.546800	-1.788324
H	0.838106	-4.559630	0.988309
H	0.966369	-0.925217	4.448242
H	0.826723	1.845903	4.363941
H	-1.363622	-2.532407	2.598950
H	0.584471	-2.929236	2.940263
H	-0.451260	-2.090868	-2.336118
H	-0.281837	2.346696	1.893312
Fe	-1.221116	-0.037068	-0.037110